This is a preprint, the final version is subject to change, of the American Mineralogist (MSA)
Cite as Authors (Year) Title. American Mineralogist, in press.
DOI: https://doi.org/10.2138/am-2019-7054

Revision 1

Geochemistry of phosphorus and the behavior of apatite during crustal anatexis: insights from melt inclusions and nanogranitoids

Chris Yakymchuk
Department of Earth and Environmental Sciences, University of Waterloo, Waterloo, Ontario, Canada, N2L 3G1

Antonio Acosta-Vigil
Instituto Andaluz de Ciencias de la Tierra, Consejo Superior de Investigaciones Científicas-Universidad de Granada, Armilla, Granada, Spain, 18100

Abstract

The solubility of apatite in anatectic melt plays an important role in controlling the trace element compositions and isotopic signatures of granites. The compositions of glassy melt inclusions and nanogranitoids in migmatites and granulites are compared with the results of experimental studies of apatite solubility in order to evaluate the factors that influence apatite behavior during prograde suprasolidus metamorphism and investigate the mechanisms of anatexis in the continental crust. The concentration of phosphorus in glassy melt inclusions and rehomogenized nanogranitoids suggests a strong control of melt aluminosity on apatite solubility in peraluminous granites, which is consistent with existing experimental studies. However, measured concentrations of phosphorus in melt inclusions and nanogranitoids are generally inconsistent with the concentrations expected from apatite solubility expressions based on experimental studies. Using currently available nanogranitoids and glassy melt inclusion compositions, we identify two main groups of inclusions: those trapped at lower temperature and showing the highest measured phosphorus concentrations, and melt inclusions trapped at the highest temperatures having the lowest phosphorus concentrations. The strong inconsistency between measured and experimentally predicted P concentrations in higher temperature samples may relate to apatite exhaustion during the production of large amounts of peraluminous melt at

high temperatures. The inconsistency between measured and predicted phosphorus concentrations for the lower-temperature inclusions, however, cannot be explained by problems with the electron microprobe analyses of rehomogenized nanogranitoids and glassy melt inclusions, sequestration of phosphorus in major minerals and/or monazite, shielding or exhaustion of apatite during high-temperature metamorphism, and apatite–melt disequilibrium. The unsuitability of the currently available solubility equations is probably the main cause for the discrepancy between the measured concentrations of phosphorus in nanogranites and those predicted from current apatite solubility expressions. Syn-entrapment processes such as the generation of diffusive boundary layers at the mineral–melt interface and adsorption of elements onto the surface of growing crystals may be responsible for concentrations of P in nanogranites and glassy melt inclusions that are higher than those predicted in apatite-saturated melt.

Key words: Apatite, phosphorus, partial melting, migmatite, granulite, melt inclusion, nanogranite

Introduction

The behavior of apatite during metamorphism is important for geochemical studies of granites (e.g. Ayres and Harris 1997; Zeng et al. 2005; Farina and Stevens 2011) and geochronology of metamorphic and metasomatic processes (e.g. Corfu and Stone 1998; Engi 2017; Kirkland et al. 2018; Bosse and Villa 2019). Because apatite hosts most of the P in metapelites and migmatites (London et al. 1999; Yakymchuk et al. 2018) it also influences the behavior of metamorphic monazite (Johnson et al. 2015; Yakymchuk 2017) and plays a critical role controlling the rare earth element budgets of magmas that ultimately produce mineral deposits (e.g. Bea et al. 1992).

Therefore, understanding the behavior of apatite during anatexis has many implications for igneous, metamorphic and hydrothermal systems.

Studies of the chemical differentiation of the continental crust and petrogenesis of migmatites and granulites rely on the composition of primary melt derived from anatexis – these melt compositions are the starting point for such studies (Sawyer 2008). The compositions of primary anatectic melts have been determined from experiments, the compositions of leucosome in migmatites, phase equilibria modeling, and from the analysis of glassy melt inclusions and nanogranitoid inclusions in peritectic minerals from migmatites and granulites (Cesare et al. 1997, 2009, 2015; Bartoli et al. 2016; Acosta-Vigil et al. 2010, 2017). Experimental studies provide fundamental benchmarks of primary melt compositions, but they are generally time consuming and the applicability of the relatively simple chemical systems to large and more complex natural systems is not always clear (White et al. 2011). Leucosomes in migmatites can represent *in situ* products of anatexis, but they rarely record primary melt compositions because they are prone to compositional variation during melt extraction and cooling of the system, such as fractional crystallization and processes associated with melt–residuum separation (e.g. Sawyer 1987; Brown et al. 2016; Yakymchuk et al. 2019). Phase equilibria modeling can allow many scenarios to be tested relatively quickly, but thermodynamic datasets are commonly extrapolated from the foundational experimental data using natural phase assemblages, and this modeling can have difficulty reproducing natural parageneses (e.g. Pattison et al. 2011; Bartoli 2017; Forshaw et al. 2019). In addition, modeling that includes phosphate minerals is very limited (e.g. Kelsey et al. 2008; Yakymchuk et al. 2017; Yakymchuk 2017; Yakymchuk and Brown 2019; Shrestha et al. 2019), and activity–composition models that include phosphorus are in their infancy (e.g. Spear 2010; Spear and Pyle 2010).

There is an increasing number of studies on glassy melt inclusions and rehomogenized nanogranitoid inclusions present in peritectic minerals from migmatites and granulites, covering various bulk rock compositions and host minerals (e.g. Cesare et al. 2015; Bartoli et al. 2016). Melt inclusions trapped by peritectic minerals generated during crustal anatexis represent, by definition, samples of the primary melts (Cesare et al. 2011, 2015; Bartoli et al. 2014). However, the results of these studies have not been yet applied to evaluating the geochemistry of phosphorus during anatexis, which has implications for the behavior and role of apatite and monazite in peraluminous granites and metasedimentary migmatites. Considering that many of the reported melt inclusions and nanogranitoids are spatially associated with apatite, (Cesare 2008; Fererro et al. 2012; Fererro et al. 2015) and that apatite itself does sometimes host tubular melt inclusions (Cesare et al. 2011), the composition of glassy melt inclusions and rehomogenized nanogranitoid inclusions can be used to test current experimental models of apatite solubility and investigate the mechanisms of anatexis in crustal rocks.

Here, we use the large dataset of the previously published glassy melt inclusions and nanogranitoids compositions (~580 analyses; Bartoli et al. 2016) to test the validity of the predictions of laboratory experiments on the solubility of apatite, and to investigate the controlling factors on phosphorus solubility in apatite-saturated melts. We identify some discrepancies between the melt inclusion and nanogranitoid dataset with experimentally-derived solubility equations for apatite in granitic (*s.l.*) melt, and discuss implications for the geological significance of melt inclusion compositions, the suprasolidus behavior of apatite, mechanisms of crustal anatexis, and linking granites to their source rocks.

Apatite solubility

The concentration of phosphorus in anatectic melt is controlled by the growth and breakdown of phosphate minerals, and, to a lesser extent, the behavior of phosphorus-rich silicate minerals. The dominant repository of phosphorus in migmatites is apatite, which is expected to exert a first-order control on the phosphorus concentration of anatectic melt and the geochemistry of P during crustal anatexis (e.g. Spear and Pyle 2002). Experimental studies have concluded that apatite solubility in melt is controlled by chemical and physical factors, including: temperature, pressure, melt composition and kinetics (Watson 1979; Watson and Green 1981; Piccoli and Candela 2002). Apatite solubility does not appear to be sensitive to H_2O content, whereas monazite—a significant repository of phosphorus in high-grade aluminous metamorphic rocks—is more sensitive (Stepanov et al. 2012). Several studies have examined these factors for apatite solubility (e.g. Harrison and Watson 1984; Bea et al. 1992; Pichavant et al. 1992; Wolf and London 1994; Toplis and Dingwell 1996; London et al. 1999).

Harrison and Watson (1984; HW84) used partial melting experiments to show that the solubility of apatite is related to temperature and the SiO_2 concentration of melt by the following relationship:

$$lnD_P^{apatite/melt} = \left[\frac{(8400+\left((SiO_2-0.5)2.64\times10^4\right)}{T}\right] - [3.1 + 12.4(SiO_2 - 0.5))] \qquad (1)$$

where SiO_2 is the weight fraction in the melt and T is in Kelvin. This relationship is predicted to be valid for melt with SiO_2 concentrations between 45% and 75 wt.%, for 0% to 10% wt.% H_2O and the range of pressures expected in the crust (Harrison and Watson 1984).

Pichavant et al. (1992; P92) demonstrated that apatite solubility increases for peraluminous melt compositions compared with metaluminous and peralkaline melts. These authors derived the following equations for P_2O_5 solubility in peraluminous melt:

$$P_2O_5^{PMR} = P_2O_5^{HW} + P_2O_5^{PER} \qquad (2)$$

This is a preprint, the final version is subject to change, of the American Mineralogist (MSA)
Cite as Authors (Year) Title. American Mineralogist, in press.
DOI: https://doi.org/10.2138/am-2019-7054

$$P_2O_5^{PER} = \left(\frac{A}{CNK} - 1\right) \exp\left(\frac{\alpha}{T} + \beta SiO2 + \gamma\right) \quad (3)$$

where, α, β, and γ are constants, T is in Kelvin, SiO_2 is the weight fraction of silica in the melt and $P_2O_5^{HW}$ is the concentration of P_2O_5 from the HW84 expression.

Bea et al. (1992; B92) produced a model based on the experimental data of Holtz and Johannes (1991) and Harrison and Watson (1984) that includes an expression for the aluminosity of the melt as follows:

$$P_2O_5^{corrected} = P_2O_5^{HW} + e^{factor} \quad (4)$$

$$e^{factor} = (ASI - 1) \times \left(\frac{6420}{T}\right) \quad (5)$$

where T is in Kelvin and ASI (aluminum saturation index) is defined as molar Al_2O_3 / [Na_2O + K_2O + CaO].

Wolf and London (1994; WL94) derived a simple linear equation that relates the aluminum saturation index of the melt to the P_2O_5 concentration of melt in chemical equilibrium with apatite:

$$P_2O_{5\ (wt.\%)} = -3.4 + 3.1 \times ASI \quad (6)$$

However, their experiments were restricted to low pressure (2 kbar) and peraluminous melt compositions (ASI > 1.1), which may be applicable for partial melting of aluminous metasedimentary rocks but not for intermediate to basic rocks.

Tollari et al. (2006) combined experimental results with published data to demonstrate an important control of CaO on the solubility of phosphorus in melt:

$$M_{P2O5}^{liq-sat} = \exp\left[T\left(\frac{-0.8579}{139.00 - M_{SiO2}^{liq}} + 0.0165\right) - 3.333\ln(M_{CaO}^{liq})\right] \quad (7)$$

where M is the molar percentage of oxides and T is in Kelvin. This model can be applied to wt.% concentrations using the following conversion factors from Tollari et al. (2006): $SiO_{2\ (mol\%)} = 1.11$

This is a preprint, the final version is subject to change, of the American Mineralogist (MSA)
Cite as Authors (Year) Title. American Mineralogist, in press.
DOI: https://doi.org/10.2138/am-2019-7054

x $SiO_{2\ (wt\%)}$; $CaO_{(mol\%)}$= 1.18 x $CaO_{(wt\%)}$; $P_2O_{5\ (mol\%)}$= 0.47 x $P_2O_{5\ (wt\%)}$. However, the effect of the CaO concentration of the melt on P_2O_5 saturation is relatively minor for granitic systems. Considering that the analyzed nanogranitoids are mostly granitic (*sensu stricto*), this expression is excluded from the analysis below.

Data handling and methodology

All of the data used in this study is from the compilation of Bartoli et al. (2016), which includes measurements of rehomogenized nanogranitoid and glassy melt inclusion compositions from various rock types (mostly metapelites and, to lesser extent, metaluminous to moderately peraluminous quartzofeldspathic rocks) from several migmatite terranes and xenoliths in volcanic rocks (Cesare et al. 2003, 2007, 2009; Acosta-Vigil et al. 2007; Bartoli et al. 2013a, b, c, 2015; Ferrero et al. 2011, 2012, 2014, 2015; Carosi et al. 2015). Apatite is a common accessory mineral in the migmatites investigated in this study (e.g. Acosta-Vigil et al. 2010) as well as in metapelites in general (Spear and Pyle 2002). In addition, apatite is commonly spatially associated with nanogranites in host peritectic minerals (e.g. Cesare 2008; Bartoli et al. 2013, Fererro et al. 2012; Fererro et al. 2015), and hence it reasonable to infer that apatite was present during suprasolidus metamorphism in the samples included in the database of Bartoli et al. (2016) that we use here. Melt inclusions and nanogranitoid compositions studied here are hosted by garnet and, more rarely, plagioclase, cordierite, quartz and ilmenite (Bartoli et al. 2016), and the minor differences in the composition of the inclusions are explored in the discussion. The estimated *P–T* conditions of the nanogranitoid and melt inclusion entrapment, along with the experimental conditions from apatite solubility studies, are summarized in Figure 1.

Concentrations of major elements were collected via electron probe microanalysis (EPMA) in various laboratories (see Bartoli at al. 2016). For 83 out of 580 analyses in Bartoli et al. (2016), concentrations of P_2O_5 were not reported, and these analyses are excluded here. The main limitation of using phosphorus data from the rest of the analyses is that ~10% of these yielded concentrations of P_2O_5 below the limit of detection. In most routine wavelength-dispersive electron probe microanalysis studies, the detection limit is inferred to be ~0.01 wt.% (or 100 ppm) P_2O_5. The statistical treatment of these values is essential for a robust analysis of the concentration data (e.g. Grunsky 2010), i.e. analyses whose P_2O_5 concentrations are below the limit of detection are still useful even though their absolute values are not known. For a robust statistical analysis of the data, values below detection have assigned concentrations based on the distribution of the dataset following the methodology of Palarea-Albaladejo and Martin-Fernandez (2015). The zCompositions package in the statistical software *R* (including the multLN function) was used. This implements a multiplicative lognormal imputation of left-censored values, such as values below the limit of detection (e.g. Palarea-Albaladejo and Martin-Fernandez 2013). Based on this approach, 52 values that were reported as below detection in Bartoli et al. (2016) were assigned a value of 0.008 wt.% P_2O_5 for the purposes of plotting in this study.

The predicted concentration of P_2O_5 in apatite-saturated melt based on the four solubility equations, was determined using the estimated temperature of entrapment (based on petrology and thermobarometry and, in the case of nanogranitoids, on the experimental rehomogenization temperature as well; see Cesare et al. 2015, and references therein), combined with the major element concentrations (SiO_2, Al_2O_3, Na_2O, K_2O, CaO) of the rehomogenized nanogranites or glassy melt inclusions measured via EPMA. The apatite solubility expression of Harrison and

This is a preprint, the final version is subject to change, of the American Mineralogist (MSA)
Cite as Authors (Year) Title. American Mineralogist, in press.
DOI: https://doi.org/10.2138/am-2019-7054

Watson (1984) requires a value for the amount of P_2O_5 in apatite to calculate the concentration of P in an equilibrated melt, whereas the other apatite solubility equations were developed to calculate this value directly. Substitution of LREE and other cations can reduce the amount of P_2O_5 in apatite. In general, the concentration of P_2O_5 in apatite ranges from 39 to 42 wt.% (Pan and Fleet 2002). REE-rich apatite can have concentrations of P_2O_5 down to ~34 wt.% (Pan and Fleet 2002). Here, we use a value of 41 wt.% P_2O_5 in apatite, which is an average of the compositions reported in Webster and Piccoli (2015).

Results

Comparison between measured and experimentally predicted P_2O_2 concentrations

Figures 2 to 4 show different ways of comparing the measured versus experimentally predicted P_2O_5 concentrations of melt inclusions in migmatites and granulites. Given that the solubility of apatite in anatectic melt is expected to be a function of several variables, we start with comparing (Fig. 2) the measured concentrations of P_2O_5 in rehomogenized nanogranites and glassy melt inclusions, along with the predicted concentrations based on the relatively simple apatite solubility expressions of Harrison and Watson (1984) and Wolf and London (1994), for a variety of SiO_2 concentrations, temperatures and values of ASI in the melt. Thus, Fig. 2 compares the experimentally predicted combinations among P_2O_5, SiO_2, temperature and ASI for the chosen range of values (SiO_2, 60–80 wt.%; temperature, 650–1000 °C; ASI, 1.1–1.4; red discontinuous lines in the diagrams), versus measured (by EPMA) P_2O_5, SiO_2 and ASI in the melt inclusions and associated temperatures obtained from petrology/geothermobarometry/experimental rehomogenization (all data coming from Bartoli et al. 2016, and references therein). Roughly 90% of the measured values from rehomogenized nanogranites and melt inclusions have

This is a preprint, the final version is subject to change, of the American Mineralogist (MSA)
Cite as Authors (Year) Title. American Mineralogist, in press.
DOI: https://doi.org/10.2138/am-2019-7054

concentrations of SiO_2 between 70 and 76 wt.% (Fig. 2a) and ASI values between 1.0 and 1.4 (Fig. 2b). For each of the investigated localities, there is a relatively large scatter in the concentrations of P_2O_5 and SiO_2 as well as ASI values. For example, melt inclusions from the El Hoyazo enclaves have concentrations of SiO_2 mostly ranging from 70–76 wt.%, ASI values between 1.0 and 1.4, and concentrations of P_2O_5 varying from <0.1 to 0.5 wt.%. As a whole, the data do not follow the T–SiO_2 trends of the Harrison and Watson (1984) solubility expression over a range of temperatures, and most plot at higher P_2O_5 values than predicted by this solubility expression (Fig. 2a). However, the data do tend to cluster in Figure 2b around the line representing the solubility expression of Wolf and London (1994), that is related to the ASI of the melt and is independent of temperature.

Because the solubility of apatite is expected to be a complex function of temperature and melt composition (Harrison and Watson 1984; Pichavant et al. 1992; Bea et al. 1992; Wolf and London 1994), the theoretical saturation concentration of P_2O_5 with respect to apatite in each of the rehomogenized nanogranite and glassy melt inclusion was calculated from the measured (by EPMA) values of SiO_2, Al_2O_3, CaO, Na_2O and K_2O, combined with the estimated entrapment temperature from each locality. This allows for a comparison of the measured versus estimated (for an apatite-saturated system) concentrations of P_2O_5 in individual rehomogenized nanogranites and melt inclusions. The calculated concentrations of P_2O_5 from each of the solubility expressions are plotted against the measured amount of P_2O_5 (wt.% from EPMA) from individual rehomogenized nanogranites or melt inclusions in Figure 3. Points plotting below the 1:1 line indicate that the measured concentrations of P_2O_5 are greater than the predicted values using the four apatite solubility expressions, measured concentrations of SiO_2, Al_2O_3, CaO, Na_2O and K_2O, and estimated entrapment temperatures. Points plotting above this line indicate that the

measured values of P_2O_5 are lower than those calculated from the solubility expressions. To further compare the measured versus calculated values, the log-normalized ratios of the measured concentrations of P_2O_5 versus predicted concentrations of P_2O_5 are plotted as histograms in Figure 4.

The expressions of Harrison and Watson (1984) and Bea et al. (1992) mostly underestimate the P_2O_5 concentration of apatite-saturated melt (Figs. 2–4). For example, the HW84 solubility model underestimates >90% of the P_2O_5 values in the nanogranitoids and melt inclusions (Fig. 4a) and the B92 solubility model underestimates ~70% (Fig. 4b). The P92 solubility expression overestimates the concentration of P_2O_5 (Fig. 4c) for most samples, except for the particular case of the metaluminous La Galite glassy melt inclusions. The WL94 model does not systematically under- or overestimate the measured P_2O_5 values (Fig 4d); however, there is no clear correlation between measured and predicted values indicating that, although measured P_2O_5 concentrations tend to follow the WL94 model trend (Fig. 2b), this model has limited predictive power (Fig. 3d).

For specific sample suites, rehomogenized nanogranitoids from the highest temperature rocks such as the Bohemian massif and the Kerala Khondalite belt (Fig. 1), are systematically overestimated for each of the four solubility expressions (Fig. 3). For the other locations, the HW84 and B92 expressions mostly underestimate the concentrations of P_2O_5, the P92 expression overestimates most of the measured values, whereas WL94 neither systematically under- nor overestimates the measured P_2O_5 (Figs. 3, 4).

Two groups of melt inclusions based on P_2O_5 concentrations and entrapment temperatures

This is a preprint, the final version is subject to change, of the American Mineralogist (MSA)
Cite as Authors (Year) Title. American Mineralogist, in press.
DOI: https://doi.org/10.2138/am-2019-7054

The distributions of the concentrations of P_2O_5 in nanogranitoids and melt inclusions separated by location and published temperatures of entrapment are summarized in Figure 5. With the exception of metaluminous melt inclusions from metatonalites in La Galite, melt inclusions and nanogranitoids with entrapment temperatures ≤825 °C have high median P_2O_5 values (~0.15–0.25 wt.%), whereas the highest-temperature samples yield low (<0.2 wt.%) concentrations of P_2O_5.

Discussion

None of the available experimental models consistently predict the measured P_2O_5 concentrations of the rehomogenized nanogranitoids and glassy melt inclusions. There is a weak correlation between phosphorus concentration and ASI (Fig. 2b), which has also been observed in experimental studies (Mysen et al. 1981; Mysen 1998; Wolf and London 1994), but none of the apatite solubility models accurately predict P_2O_5 concentration in the studied nanogranitoids and glassy melt inclusions (Fig. 3, and in particular Fig. 3d). The inconsistency between the measured and predicted phosphorus concentrations of inclusions from solubility equations may result from several factors and processes. Some of these factors/processes could explain why measured P_2O_5 concentrations are lower than predicted (i.e. overestimation of P_2O_5 by models, mostly applicable to the highest-T, lowest-P_2O_5 melt inclusions), including: (1) challenges associated with EPMA of rehomogenized nanogranitoids and melt inclusions; (2) sequestration of P by substitution in major minerals; (3) sequestration of P by crystallization of monazite due to saturation of LREE in melt during apatite dissolution; (4) unavailability of apatite, either by inclusion of apatite in major minerals or complete apatite dissolution; and (5) disequilibrium during anatexis or rapid entrapment of melt inclusions before matrix melt–residuum

equilibration. Other factors/processes may explain why measured P_2O_5 concentrations are higher than predicted that are most relevant for the lowest-T, highest-P_2O_5 melt inclusions include: (6) unsuitability of the solubility equations at the *P–T–X* conditions of melt entrapment; (7) measured melt compositions may not reflect those of the matrix melt at the time of entrapment, due to syn- and/or post-entrapment processes. Each of these possibilities is discussed below, followed by a more detailed assessment using the large data set of melt inclusions from the El Hoyazo enclaves. We acknowledge that these processes may work against each other with respect to the concentration of phosphorus in anatectic melt, but comparing the measured versus predicted values of P_2O_5 in rehomogenized nanogranites and melt inclusions provides a first-order assessment of the potential importance of each process. Afterwards, we discuss some implications for studies of granite petrogenesis.

Electron probe microanalysis of rehomogenized nanogranitoid and glassy melt inclusions

Homogenized melt inclusions in peritectic host minerals are usually very small with diameters of <20 μm, which makes EPMA difficult (Bartoli et al. 2016). EPMA analysis of these tiny inclusions requires in most cases a small beam size (~1 μm), which can lead to the loss of Na and possibly K during excitation (Morgan and London 2005; Ferrero et al. 2012). Consequently, the concentrations of K and Na in the measured glassy melt inclusions and rehomogenized nanogranitoids may be lower than true values, producing artificially higher ASI values.

While this is not expected to have a large impact on the measured concentration of SiO_2, which is essential for the HW84 solubility model, it may result in slightly higher ASI values, which are important in the solubility expressions of P92, B92 and WL94. For the WL94 solubility expression, there is no systematic offset of the measured values from the predicted

values for P_2O_5 (Fig. 4d). The P92 solubility expressions mostly overestimate the concentration of P_2O_5 in the nanogranitoids and melt inclusions, whereas B92 mostly underestimate it except for the highest-T samples from Bohemian Massif and Kerala Khondalite. Hence the potential loss of alkalis during the EPMA of the melt inclusions might explain the inconsistency regarding the P92 model and values for the highest-temperature inclusions predicted by B92. However, considering that the analysis of nanogranitoids and melt inclusions used secondary glass standards to correct for the loss of alkalis as recommended by Morgan and London (2005), we conclude that K and Na migration during EPMA is not expected to be the principal cause of the deviation between measured and predicted concentrations of P_2O_5 in melt inclusions and nanogranitoids.

Due to the small size of melt inclusions, the excitement volume during EPMA may include parts of the host minerals. The effect of this would include an analytical mix between the two. Most melt inclusions are hosted by garnet, which can have concentrations of P up to a few hundred ppm (Kohn and Malloy 2004; Pyle and Spear 1999), which is near the detection limit of ~100 ppm for P_2O_5 in routine analyses. Most analyses of P_2O_5 in melt inclusions are >>100ppm. In the hypothetical case that the analysis of nanogranitoid inclusions results in a mix of homogenized glass and the relatively P-poor host mineral (e.g. garnet), then measured values will be slightly lower than predicted values from the solubility equations. In addition, a mixed analysis between garnet and the rehomogenized nanogranites or melt inclusions could yield an artificially elevated ASI value that would overestimate the calculated concentration of P_2O_5 in apatite-saturated melt (except for the HW84 apatite solubility model). Both of these scenarios would result in calculated values of P_2O_5 in apatite-saturated melt that are higher than the measured values, which is not observed in most cases (Fig. 3). Furthermore, the concentrations

of FeO and MgO in the measured nanogranitoids and melt inclusions are too low to have included a significant component of garnet in the analyses (Bartoli et al. 2016). Therefore, mixed analyses alone cannot account for the discrepancies between the measured and predicted concentrations of P_2O_5 in the rehomogenized nanogranites and melt inclusions.

Sequestration of P by partitioning into major minerals

The growth and consumption of the major rock-forming minerals can affect the stability of apatite, mostly by partitioning P during their growth, which may decrease the effective concentration of P in the system and enhance apatite consumption during partial melting. Apatite is generally considered to represent the main repository for P in migmatites (e.g. London et al. 1999). However, major rock-forming silicate minerals can accommodate a significant proportion of the P budget during metamorphism (e.g. Spear and Pyle 2002). In most metasedimentary migmatites, garnet can represent a significant sink for P with concentrations of a few hundred ppm (Kohn and Malloy 2004; Pyle and Spear 1999; Acosta-Vigil et al. 2010). Plagioclase is common in metasedimentary and most igneous migmatites and can accommodate several hundred ppm of P (e.g. Villaseca et al. 2003; Acosta-Vigil et al. 2010; Dumond et al. 2015). Alkali feldspar can also accommodate significant amounts of P in strongly peraluminous melt (London 1992; London et al. 2012). A simple mass balance calculation by Yakymchuk et al. (2018) indicates that garnet and plagioclase can host up to ~20% of the P budget in an average metapelite. During suprasolidus prograde metamorphism in metapelites, plagioclase is generally expected to be produced from the wet solidus up to muscovite exhaustion (Yakymchuk & Brown 2014; Yakymchuk et al. 2017). K-feldspar is predicted to grow during muscovite and biotite-

breakdown melting, and is consumed at high-temperatures above the stability of biotite. Garnet is expected to grow during biotite-breakdown melting.

Figure 6 is a *P–T* diagram showing the amount of apatite dissolution for an average metapelite composition in a closed system (i.e. no melt loss or gain), using the WL94 solubility expression and considering the simple scenario where apatite is the only repository of P. Between the wet solidus and biotite out, apatite dissolution is required to saturate the increasing proportion of melt. If P substitutes into major minerals, then the dissolution contours on Figure 6 will shift to lower temperatures. Consequently, apatite exhaustion is more likely to occur at lower temperatures in garnet- and feldspar-rich migmatites.

The incorporation of P into major minerals would therefore decrease the concentration of P in the reaction volume or effective bulk composition, to the point of producing the exhaustion of apatite at lower temperatures. If this is the case, however, models would overestimate the P_2O_5 concentration in the nanogranitoids and melt inclusions, contrary to what we observe, except for model P92 and perhaps the highest-temperature samples for models HW84 and B92 (Figs. 3 and 4).

Sequestration of P by crystallization of monazite

Dissolution of apatite in strongly peraluminous melt can result in concomitant crystallization of monazite at the apatite–melt interface (Wolf and London 1995; Wolfram et al. 2017), due to the relative solubilities of apatite and monazite in peraluminous granite melts (the solubility of apatite and monazite increases and decreases, respectively, in peraluminous melt at constant temperature). The current melt inclusion dataset includes mostly moderate to strongly peraluminous melts (Fig. 2b) and, therefore, it is possible that monazite crystallized during the

dissolution of apatite into the matrix melt of the host anatectic rocks. In this scenario, a portion of P coming from the dissolution of apatite would have been sequestered into the crystallizing monazite, moving the dissolution contours of Fig. 6 towards lower temperatures. Consequently, crystallization of P-rich accessory minerals (e.g. monazite) will also reduce the stability of apatite at high temperatures and may ultimately result in early apatite exhaustion and melt that is undersaturated in P.

Abundance and microstructural location of apatite

Measured concentrations of P_2O_5 in melt inclusions and nanogranitoids are generally higher at lower temperature and lower at UHT conditions (Fig. 5), except for metatonalite samples from La Galite. This contrasts with the general positive temperature-dependence of apatite solubility determined from experimental studies. Two possible explanations for this discrepancy are that apatite became exhausted in the migmatites and granulites at high temperature due to (i) progressive increase in the proportion of melt with or without P substitution into peritectic minerals, or (ii) the physical isolation of apatite away from the reaction volume.

The ASI of anatectic melt is predicted to increase during heating above the solidus in an equilibrated system (Johnson et al. 2015; Yakymchuk et al. 2017; Yakymchuk 2017). Between the wet solidus and biotite out, apatite dissolution is required to saturate the increasing proportion of progressively more peraluminous melt. Hence at very high-temperature conditions, apatite exhaustion may be caused by progressive partial melting and apatite dissolution (Fig. 6). For example, Nandakumar and Harley (2019) estimate that migmatites in the Kerala Khondalite belt have lost ~30% melt, which may have been enough to consume most apatite (c.f. Yakymchuk 2017). At increasing temperatures above apatite exhaustion, the concentration of P

in the melt will decrease due to the breakdown of P-poor minerals and progressive dilution (Fig. 7). In general, if apatite exhaustion is the primary reason for the discrepancy between measured and predicted P_2O_5 concentrations, each solubility model would overestimate P_2O_5 in the nanogranitoids and melt inclusions, and this is not observed (Figs. 3 and 4). Only the P92 solubility expression consistently overestimates concentrations of P_2O_5 in nanogranitoids (Fig. 4c). The highest temperature samples from the Bohemian Massif, the Kerala Khondalite belt and the Barun gneisses (Figs. 1 and 5) are broadly metapelitic in composition and the solubility of apatite is expected to increase with increasing temperature and melt ASI. Considering that apatite may become exhausted at high temperature, it is possible that apatite was locally completely consumed and further melting resulted in the dilution of the melt in P_2O_5 (Fig. 7). In this scenario, the concentration of P_2O_5 in the melt trapped by growing peritectic minerals is expected to be lower than for apatite-saturated melt. The systematic overestimation of P_2O_5 in melt inclusions for these samples by all experimental models suggests that the discrepancy between measured and predicted P_2O_5 concentrations might be due to apatite exhaustion for the particular cases of the highest temperature rocks. This process does not likely explain, however, the overestimation of P by B92 and WL94 in part of the lower-T melt glassy inclusions and nanogranitoids, or by P92 in all of the lower-T melt inclusions and nanogranitoids.

Sequestration of apatite away from the reaction volume by inclusion into residual or peritectic minerals decreases the effective concentration of P in the system. This would also reduce the amount of apatite available to the melt and may result in early (i.e. low *T*) apatite exhaustion relative to the closed-system equilibrium model in Figure 6. However, previously conducted microstructural studies in migmatites have concluded that accessory minerals tend to be located at grain boundaries, particularly those with larger grain sizes (Watson et al. 1989; Bea

1996); therefore, accessory minerals are generally expected to be accessible to the melt. Consequently, apatite sequestration is not expected to be the primary cause of the discrepancy between measured and predicted concentrations of phosphorus in nanogranites and glassy melt inclusions.

Disequilibrium

The dissolution of apatite into anatectic melt is sensitive to temperature and water content (Harrison and Watson 1984), and involves the diffusion of P and Ca away from the interface and the uphill diffusion of Al towards the apatite–melt interface (Wolf and London 1994). During anatexis, the timescales of melt extraction will compete with dissolution rates, which can result in undersaturated melt compositions with respect to apatite (Watt and Harley 1993; Zeng et al. 2005). Very short melt extraction rates of decades to centuries have been reported in some studies (Harris et al. 2000; Villaros et al. 2009) and are generally related to dynamic systems undergoing anatexis and deformation. The timescales of melt extraction and accessory mineral dissolution are important in studies of granites, however, melt inclusions and nanogranitoids represent melt trapped in growing peritectic minerals during melting. The extent of equilibration between this trapped melt and accessory minerals will relate to the timescales of growth of the peritectic mineral relative to the rates of dissolution of the accessory minerals and diffusion of their essential structural constituents.

The timescales of prograde metamorphism in anatectic terranes and of peritectic garnet growth, usually range from Ma to tens of Ma (e.g. Hermann and Rubatto 2003; Clark et al. 2011; Weinberg 2016). These timescales are much longer than the time expected to dissolve apatite under most geologically realistic circumstances. For example, the dissolution timescale of a 500

μm diameter apatite grain in melt with 6 wt.% H_2O at 750°C is expected to be < 1 ka (Harrison and Watson 1984). Therefore, in this scenario, it is likely that apatite equilibrates with the anatectic melt (at least locally) in high-temperature terranes. However, there are also studies concluding that the entrapment of melt inclusions by growing crystals requires growth rates of 10^{-8}–10^{-10} m/s (Baker 2008), implying growth of 5–10 mm diameter host crystals in days to years. Hence, although metamorphic cycles last Ma to tens of Ma, it is unclear how long it takes to grow porphyroblasts of the peritectic minerals in anatectic systems.

Regardless of the timescales and temperatures of partial melting, disequilibrium between apatite and melt should result in the systematic overestimation of P_2O_5 concentrations by the apatite solubility expressions. For the samples from the Kerala Khondalite belt (Cesare et al. 2009; Ferrero et al. 2012) and the Bohemian Massif (Ferrero et al. 2015), most concentrations of P_2O_5 are overestimated by the solubility expressions (Fig. 4). However, these samples also record the highest temperatures and should be least susceptible to disequilibrium because of the strong temperature dependence on apatite dissolution kinetics (e.g. Harrison and Watson 1984). An alternative and better explanation for the overestimation of concentrations of P_2O_5 in these samples, as discussed earlier, may be the exhaustion of apatite at high temperature (Figs. 6 and 7). For some of the overestimated P_2O_5 concentrations by P92, WL94 and B92 (Fig. 3), this process could also explain part of the difference between measured and predicted concentrations of P_2O_5, particularly for the case of the lowest-T melt inclusions and nanogranitoids, although the growth rate of the host minerals in each of the case studies is also a key but unknown variable.

Unsuitability of solubility equations

462 Current solubility equations for apatite in melt are based on hundreds of experimental runs over a
463 wide range of melt compositions and temperatures. The HW84 solubility equation was calibrated
464 for temperatures of 850–1500°C (Fig. 1). Melt inclusions from samples with the highest
465 temperature of entrapment (e.g. Bohemian Massif and the Kerala Khondalite belt) have
466 measured concentrations of P_2O_5 that are around or below the values predicted by the HW84
467 expression (Fig. 3a). Although the HW84 solubility expression does not consider the aluminosity
468 of the melt, it provides the closest estimates for the amount of P_2O_5 in anatectic melt at high
469 temperatures (compared to B92, P92 and WL94). However, the HW84 expression generally
470 underestimates the amount of P_2O_5 in melt inclusions from the lower temperature localities.
471 Interestingly, samples from the Bohemian Massif and Kerala Khondalite belt have some of the
472 lowest concentrations of P_2O_5 in rehomogenized nanogranites and melt inclusions, and this may
473 be due to the complete consumption of apatite as discussed earlier.

474 The B92 apatite solubility expression mostly underestimates the amount of P_2O_5 in melt
475 inclusions and nanogranitoids (Fig. 4b). One possible reason for this is that the calibration is
476 based on the experimental data of Holtz and Johannes (1991). These authors investigated melt
477 compositions with SiO_2 >75% and ASI values between 1.250 and 1.467 – most of the melt
478 inclusion data from Bartoli et al. (2016) have lower SiO_2 and ASI values (Fig. 2). In addition, the
479 B92 solubility expression is also based on the Harrison and Watson (1984) expression that was
480 calibrated using higher temperature experiments than the estimated entrapment temperatures of
481 most melt inclusions. Therefore, the B92 expression may not be appropriate for investigating
482 apatite solubility in relatively low SiO_2 and low ASI melts at temperatures <850°C.

483 The P92 solubility model predicts very high values for the concentration of P_2O_5 in
484 anatectic melt of up to 2 wt.% (Fig. 3c). The experimental results of Pichavant et al. (1992)

This is a preprint, the final version is subject to change, of the American Mineralogist (MSA)
Cite as Authors (Year) Title. American Mineralogist, in press.
DOI: https://doi.org/10.2138/am-2019-7054

485 contain glasses with wt.% concentrations of P_2O_5, and the P92 solubility expression predicts >1
486 wt.% P_2O_5 in melt even at modest ASI values. These are significantly higher than P_2O_5
487 concentrations in nanogranitoids (Fig. 2) and in peraluminous granites (e.g. Pichavant et al.
488 1992).

489 The WL94 solubility expressions coupled with the melt inclusion compositions from
490 Bartoli et al. (2016) result in roughly half of the predicted concentrations of P_2O_5 underestimated
491 and half overestimated (Fig. 4d). The WL94 expression significantly overestimates the
492 concentrations of P_2O_5 in the melt inclusions in some cases (Fig. 3d). For example, 118 melt
493 inclusions (out of 497) are predicted to have P_2O_5 concentrations >0.5 wt.% whereas only 19
494 measured melt inclusions have concentrations >0.5 wt.%.

495 Previous experimental studies have shown that temperature, concentration of SiO_2, and
496 the ASI value of the melt are three important variables controlling the solubility of apatite in
497 granitic melts. However, there is the possibility that the currently proposed relationships between
498 apatite solubility and *T*, SiO_2 and ASI values are not accurate enough, and/or that there are
499 additional variables that should be considered. Figure 8 illustrates the inconsistency of current
500 models predicting P_2O_5 concentrations in melt inclusions from the El Hoyazo anatectic enclaves
501 in the Neogene Volcanic Province of SE Spain. This difference between the measured and
502 predicted concentrations of P_2O_5 in melt among the several experimental models—which is a
503 function of ASI, weight % SiO_2 and other possible factors—can reach up to ~1.0–1.5 wt.% and is
504 largest in high-SiO_2 and high-ASI compositions. This may suggest that future experimental
505 studies should focus on investigating the solubility of apatite in strongly peraluminous, SiO_2-rich
506 melts that are analogous to evolved S-type granites. Importantly, the unsuitability of solubility

This is a preprint, the final version is subject to change, of the American Mineralogist (MSA)
Cite as Authors (Year) Title. American Mineralogist, in press.
DOI: https://doi.org/10.2138/am-2019-7054

equations is one factor that may explain the underestimation of P by models, which is mostly applicable to the lowest-T, highest-P_2O_5 glassy melt inclusions and nanogranitoids.

Compositions of melt inclusions and rehomogenized nanogranitoids

The comparison of experimentally-derived apatite solubility expressions and measured compositions of rehomogenized nanogranitoids and melt inclusions requires that the analyzed inclusions are representative of the matrix melt surrounding the growing mineral host. Melt trapped by growing peritectic minerals is primary by definition (e.g. Cesare et al. 2011, 2015; Bartoli et al. 2014), however, it might not be representative of the matrix melt composition at the time of entrapment. This may be due to melting in disconnected pockets along grain boundaries with variable interaction with apatite. In addition, syn-entrapment processes taking place at the mineral–melt interfaces and/or post-entrapment processes can both modify an originally representative matrix melt composition. Syn- and post-entrapment modification can be a major problem associated with the study and interpretation of melt inclusion compositions (Roedder 1984; Acosta-Vigil et al. 2017).

For the particular case of melt inclusions in migmatites and granulites, evaluating the significance of syn- and post-entrapment processes needs to be carefully evaluated, case by case, by acquiring, analyzing and comparing results from large and high-quality analytical datasets on many occurrences, ideally covering a variety of *P–T* conditions, host rock compositions, and geodynamic settings (Cesare and Acosta-Vigil 2011, Cesare et al. 2011). Trapping of locally derived melt in isolated equilibration domains without apatite could produce unexpectedly low P concentrations in the melt inclusions. Syn-entrapment processes could either deplete or increase the concentration of P in the melt inclusions with respect to the original matrix melt, depending

on mineral host growth rates and diffusivity and compatibility of P with respect to the host. For example, a rapidly growing mineral host combined with the slow-diffusing P (~10^{-14}–10^{-15} m^2/s in hydrous granite melt at 750–800 °C; Pichavant et al. 1992; Wolf and London 1994) could produce enrichments of this element in the interface melt up to concentrations above the currently known saturation of apatite. Post-entrapment processes could also either increase or decrease P in the melt inclusions via diffusive equilibration of P with host mineral, depending on the starting concentration of P in, and the equilibrium partition coefficient between, host and melt. Each particular case study must, therefore, be analyzed in detail to understand the potential effects of these processes.

The results from previous analyses of the currently available datasets suggest that local melting and syn- and post-entrapment processes did not control/affect the composition of trapped matrix melts regarding their major elements, volatiles and incompatible trace element concentrations; however, they seem to affect the concentrations of the compatible (with respect to the host mineral) trace elements (Acosta-Vigil et al. 2010, 2017; Bartoli et al. 2014, 2016; Cesare et al. 2015; see more details below, section on El Hoyazo). Phosphorus can generally be considered as incompatible with respect to garnet and feldspars (except when melt ASI >1.35, in which case P becomes compatible in alkali feldspars; London et al. 1993; Bea et al. 1994). Hence, measured P concentrations in melt inclusions are probably representative of the melt at the time of entrapment. However, syn- and post-entrapment processes constitute, together with the unsuitability of solubility equations, some possible explanations for the general underestimation of P in melt by current apatite solubility models (Fig. 3).

552 **Mechanisms of anatexis from the perspective of phosphorus: insights from the El Hoyazo**
553 **enclaves**

554 Taking advantage of the extensive and detailed study of melt inclusions in the El Hoyazo
555 anatectic enclaves, we now evaluate all the factors described above and provide some new
556 insights into the mechanisms of anatexis of these enclaves from the geochemistry of phosphorus.
557 Melt inclusions in the metasedimentary enclaves of the El Hoyazo peraluminous dacite (Betic
558 Cordillera, SE Spain) were trapped during anatexis of the lower continental crust of Southern
559 Iberia at ~9 Ma (Cesare et al. 2003, 2009), and were quenched to glass upon fragmentation of the
560 protolith, incorporation into the dacite magma and rapid extrusion at ~6 Ma (Zeck and Williams
561 2001), with no or rare crystallization of daughter minerals (Cesare et al. 1997; Acosta-Vigil et al.
562 2007). Previous studies have concluded that melt inclusions in minerals of El Hoyazo enclaves
563 record the evolution in the composition of the melt, and the extent of melt–residue equilibrium,
564 during prograde metamorphism and anatexis of the host metapelite from the wet solidus to
565 temperatures of ~750 °C (Cesare and Maineri 1999; Acosta-Vigil et al. 2007, 2010, 2012). As
566 for the case of all the lower-temperature (Ronda1, La Galite), and some of the high-temperature
567 (Ronda2, Kali Gandaki) nanogranitoids and glassy melt inclusions, the HW84 and B92 solubility
568 expressions mostly underestimate, P92 overestimate, whereas WL94 does not systematically
569 under- or overestimate P_2O_5 in these inclusions, when compared with measured P_2O_5
570 concentrations. The systematics of P in this case study might, therefore, be used as a proxy for
571 most analyzed nanogranitoids and melt inclusions, except for the highest-temperature, lowest-P
572 nanogranitoids.

573 **Rehomogenization and analysis of the melt inclusions**. Melt inclusions in the El
574 Hoyazo enclaves were trapped during partial melting at the base of a thinned continental crust

575 and then quenched to glass upon rapid extrusion, with no or rare crystallization of daughter
576 minerals (Cesare et al. 1997; Acosta-Vigil et al. 2007, 2010, 2012). This avoids the experimental
577 re-homogenization stage, which is necessary for accurately measuring the compositions of
578 nanogranitoids (Cesare et al. 2015). The analyzed melt inclusions were always large enough
579 (~10–30 μm) to accommodate a 5 μm EPMA beam and a 19 μm laser ablation beam,
580 minimizing or avoiding both the loss of alkali elements and contamination by the host during
581 major, minor, and trace element analyses of the glasses (Acosta-Vigil et al. 2007, 2010, 2012).
582 Nevertheless, these factors cannot explain the discrepancy between measured and calculated
583 P_2O_5 concentrations.

584 **Sequestration of P into major and accessory minerals, and extent of melt–residue**
585 **equilibrium**. The time interval between the initiation of melting and melt inclusion entrapment
586 during anatexis of El Hoyazo enclaves might have been as short as days to years (Acosta-Vigil et
587 al. 2010). This scenario is different from the rest of reported low- to high-temperature
588 nanogranitoids and melt inclusions in Bartoli et al. (2016). Hence, even if accessory minerals
589 such as apatite and monazite were available to the melt, sluggish diffusion of their components in
590 melt over these short time scales, coupled with the sequestration of P by major minerals, could
591 have contributed to the undersaturation of apatite in the melt. Therefore, we evaluate the extent
592 of apatite–melt and residue–melt equilibration by (i) determining the extent of major mineral–
593 melt equilibration, (ii) determining if melt inclusion compositions record the presence of relict
594 diffusion profiles produced during the dissolution of apatite into the melt, and (iii) comparing the
595 extent of equilibration between melt inclusions and other accessory minerals such as zircon and
596 monazite, as well as the diffusivities of their essential structural constituents (Zr, Th, LREE
597 versus P) in melt.

598 EPMA and LA-ICP-MS analyses show that minerals coexisting with melt in the El
599 Hoyazo enclaves have relatively high concentrations of P (Acosta-Vigil et al. 2012a). For
600 example, plagioclase makes up ~35–40 wt.% of the rock and has ~300–800 ppm phosphorus.
601 Garnet makes up ~10–15wt.% of the rock and has P concentrations of ~100–300 ppm. K-
602 feldspar is rare (~2–3 wt.%), but contains very high concentrations of P (~1100–1300 ppm). A
603 total of ~15–20 wt.% of P budget is estimated to have been hosted by these major minerals
604 during anatexis (Acosta-Vigil et al. 2012a, unpublished data), which is similar to estimates for an
605 average metapelite based on phase equilibrium modeling (Yakymchuk et al. 2018). Using the
606 measured concentrations of P in the minerals and the matrix glass as well as minerals and glassy
607 melt inclusions, calculated mineral–melt P concentration ratios in the enclaves are as follows:
608 plagioclase/melt inclusions in plagioclase ~0.4–0.9; garnet/melt inclusions in garnet ~0.04–0.14;
609 rims of plagioclase/matrix melt ~0.2–1.0; rims of garnet/matrix melt ~0.1–0.2 (data from Acosta-
610 Vigil et al. 2007, 2010, Acosta-Vigil et al. in preparation). These values are all similar published
611 equilibrium distribution coefficients ($K_d^{P}{}_{Pl/melt} \leq 0.90$; London et al. 1993) and concentration
612 ratios measured in migmatites ($P_{Grt}/P_{leucosome}$ ~0.01; Bea et al. 1994) and indicates that melt in the
613 enclaves (now represented by glassy melt inclusions and matrix glass) was likely at, or relatively
614 close to, equilibrium with the major mineral assemblage. Hence major minerals sequestered P
615 from, but were probably not far from equilibrium with, the melt in the El Hoyazo anatectic
616 enclaves.

617 Figure 9 shows the variation in the concentrations of P_2O_5 (~0.1–0.4 wt.% for melt
618 inclusions in plagioclase; ~0.2–0.5 wt.% for melt inclusions in garnet) and, among others, SiO_2,
619 SiO_2, CaO and ASI in the melt inclusions. Although the systematics of multicomponent diffusion
620 in granite melt are complex (e.g. Acosta-Vigil et al. 2012b, 2017), the lack of a positive

correlation between P_2O_5, CaO, Al_2O_3 and ASI, and lack of negative correlations between e.g. P_2O_5 and Si_2O, indicates that the heterogeneity shown in Fig. 9 is not a product of diffusion profiles produced by the dissolution of apatite into melt (c.f. Wolf and London 1994). Such diffusion profiles are generated through: (1) the addition of P and Ca into the melt, (2) the concomitant uphill diffusion of Al towards the apatite-melt interface, and (3) the exchange of 1(Al+P) by 1Si along the diffusion profile. The absence of covariation among these components is inconsistent with the preservation of relict diffusion profiles caused by apatite dissolution in the El Hoyazo enclaves (compare our Fig. 9 with Figs. 2, 8, 9 from Wolf and London 1994). The implication is that although matrix melt was relatively heterogeneous during anatexis in the El Hoyazo enclaves, heterogeneity was not due to partial equilibration with apatite. Moreover, residue and matrix melt was at or close to equilibrium with respect to P at least at mineral–melt interfaces (see above).

Although melt inclusions from El Hoyazo are surprisingly rich in Zr, Th and LREE considering timeframes of days to years and currently known diffusivities of HFSE and REE in granite melt (~10^{-16}-10^{-18} m^2/s at ~750 ºC; Zhang et al. 2010, and references therein), melt inclusions are slightly undersaturated with respect to zircon and monazite. Thus, calculated saturation temperatures for zircon and monazite are ~25–50 °C lower than those of the petrologically inferred melting reactions that produced the melt inclusions (Acosta-Vigil et al. 2012a). Reported diffusivities of P (~10^{-14}-10^{-15} m^2/s, hydrous granite melt, 750–800 °C: Pichavant et al. 1992; Wolf and London 1994) are about two orders of magnitude faster than Zr and REE. Considering that the melt inclusions are close to saturation with respect zircon and monazite and P diffusion is two orders of magnitude faster than the essential structural

643 constituents of these minerals (Zr, LREE), this suggests that during anatexis, melt was likely at,
644 or close to equilibrium with, apatite in the El Hoyazo enclaves.

645 **Abundance and microstructural location of apatite**. Apatite is present and relatively
646 abundant in the El Hoyazo enclaves (~0.5 wt.%, Acosta-Vigil et al. 2010). Although ~70–75
647 vol.% of accessory minerals (apatite, monazite and zircon) are included in major minerals
648 (plagioclase, garnet, biotite, cordierite, K-feldspar) of the enclaves, a large proportion of
649 accessory minerals contain melt inclusions, independent of their microstructural location. This
650 suggests that most of the accessory minerals, including apatite, interacted with the anatectic melt
651 (Acosta-Vigil et al. 2012a), and therefore that the sequestration of apatite within major minerals
652 did not play a role for any potential undersaturation of P_2O_5 in melt. Partitioning and
653 sequestration of P into major and accessory minerals, and disequilibrium between residue and
654 melt, therefore, do not seem to play a role in the concentrations of P in melt inclusions from the
655 El Hoyazo enclaves. In addition, these factors/processes cannot explain the underestimation of P
656 by most models in the lower-T nanogranitoids and glassy melt inclusions (Fig. 3).

657 **Compositions of melt inclusions**. Measured melt inclusion may not always be
658 representative of the matrix melt surrounding the growing peritectic mineral at the time of
659 entrapment. The composition of matrix melt (later trapped as melt inclusions) can be modified
660 by syn-entrapment and post-entrapment processes.

661 Syn-entrapment processes that may affect the composition of matrix melt during
662 peritectic mineral growth and melt entrapment include: (i) the generation of diffusive boundary
663 layers in the interface melt (e.g. Albarede and Bottinga 1972); and (ii) the adsorption or
664 enrichment of elements in the surface layers of rapidly growing crystals (e.g. Watson 1996). The
665 analysis of Acosta-Vigil et al. (2012a) suggests that the development of diffusive boundary

layers probably did not affect the composition of matrix melt being trapped as inclusions. However, adsorption or enrichment of elements in the surface layers around growing crystals is only expected to affect the concentrations of the compatible (with respect to the host mineral) trace elements, which appear over-concentrated in the mineral host and depleted in the melt inclusions with respect to published equilibrium partition coefficients. Phosphorus, however, is not a compatible element either in garnet or plagioclase, at least for melt with ASI values of ~1.20 and Ca-rich plagioclase (London et al. 1993), as it is the case here (Acosta-Vigil et al. 2007, 2010). Hence, the concentration of P in the measured glassy melt inclusions in the El Hoyazo enclaves is expected to be representative of the concentration in the surrounding matrix melt and was probably not substantially affected by the development of syn-entrapment processes. Nonetheless, syn-entrapment processes have the potential to generate local melt volumes with higher concentrations of P than expected in apatite-saturated melt and may be partly responsible for melt inclusions with such high concentrations of P.

Post-entrapment processes can also affect the composition of melt inclusions so that they may not be representative of the composition of matrix melt during entrapment. Two potentially significant processes include: (i) dissolution of the host mineral into the melt inclusion or crystallization of the host mineral from trapped melt, and (ii) diffusive exchange of elements between the host mineral and the melt inclusion. Melt inclusions from El Hoyazo were trapped at ~10–100 °C above the wet solidus and, after entrapment, the temperature of the enclaves increased ~50–150 °C (Acosta-Vigil et al. 2010). Consequently, the host mineral may have either dissolved into, and/or crystallized from, the melt. However, both compositional trends for melt inclusions from individual enclaves, and lack of daughter minerals in the glassy melt inclusions, show that this is not the case (Acosta-Vigil et al. 2007, 2012a). Therefore, host mineral

689 dissolution or crystallization is not expected to have influenced the composition of glassy melt
690 inclusions in the El Hoyazo enclaves.

691 Post-entrapment diffusive exchange of P between melt inclusions and host minerals
692 (garnet and plagioclase) could have also modified the original composition of trapped melts,
693 particularly considering the small size of the inclusions (a few micrometers across) compared to
694 the large size of the hosts (millimeter-sized crystals). The extent of this exchange will depend on
695 the time the system is at high temperature and the extent to which the ratio of P in the crystal to
696 the melt inclusions deviates from an equilibrium distribution. Given that (i) there are no
697 preserved diffusion profiles from the melt inclusion to the host mineral in the samples
698 investigated by Acosta-Vigil et al. (2012a), (ii) host minerals and melt inclusions are at or close
699 to equilibrium with respect to P (see above), and (iii) currently available information on the
700 effects of temperature and composition on the equilibrium distribution coefficient of P between
701 minerals and melt is very scarce (London et al. 1993; Bea et al. 1994), we conclude that if post-
702 entrapment diffusional exchange between trapped melt and host mineral occurred, they were
703 minor. Therefore diffusion of P in/out of the melt inclusions does not seem to be a factor
704 explaining differences between measured and experimentally predicted P concentrations.

705 As a corollary, although the effects of syn- and post-entrapment processes on the
706 composition of trapped melts require further investigation (particularly the potential
707 accumulation of P at the mineral–melt interface during the generation of diffusive boundary
708 layers), none of the above factors alone account for the differences between measured and
709 predicted P_2O_5 concentrations in the analyzed melt inclusions. The potential unsuitability of
710 current experimental models seems to explain at least some of the discrepancy for the case of the
711 lowest-temperature, highest-P concentrations melt inclusions (Fig. 8).

This is a preprint, the final version is subject to change, of the American Mineralogist (MSA)
Cite as Authors (Year) Title. American Mineralogist, in press.
DOI: https://doi.org/10.2138/am-2019-7054

712 **Mechanisms of anatexis**. The above analysis suggests that the studied El Hoyazo
713 anatectic system was likely at or close to equilibrium with respect to P. This includes equilibrium
714 concentrations of P in the major minerals as well as melt (now entrapped) that was close to
715 saturation with respect to apatite. Evidence for approximate equilibrium in the anatectic system
716 includes: (i) melt inclusions are close to saturation with respect to zircon and monazite, whose
717 essential structural constituents (Zr, LREE) diffuse slower in the melt with respect to P; (ii) melt
718 heterogeneity is not related with concentration profiles produced by the diffusive dissolution of
719 apatite (see above); and (iii) most experimental models underestimate P in these melt inclusions
720 (Fig. 3). Incorporation of P into the major minerals may have occurred either by destabilization
721 of apatite inclusions (see fig 8 of Acosta-Vigil et al. 2010) or through interaction with the matrix
722 melt, via dissolution of apatite into (and diffusion of P through) the melt and, likely,
723 recrystallization of the major minerals through the melt (see Cesare and Maineri 1999; Acosta-
724 Vigil et al. 2010).

725 Even though glassy melt inclusions from the El Hoyazo enclaves were likely in
726 equilibrium with the anatectic system (including concentrations P_2O_5), the compositions are
727 variable and this suggests that matrix melt was heterogeneous at the time of entrapment (Acosta-
728 Vigil et al. 2007, 2017, and Fig. 9). The presence of variable matrix melt compositions during
729 anatexis is also supported by the heterogeneity of normative Qtz-Or-Ab compositions of melt
730 inclusions from the enclaves (see Acosta-Vigil et al. 2012b, 2017). In the particular case of P_2O_5,
731 and based on the currently available experimental studies, P_2O_5 variability in melt in anatectic
732 systems may be associated with local heterogeneities in SiO_2 and ASI in the melt (Fig. 9), and
733 not with variable degrees of apatite undersaturation in the melt.
734

This is a preprint, the final version is subject to change, of the American Mineralogist (MSA)
Cite as Authors (Year) Title. American Mineralogist, in press.
DOI: https://doi.org/10.2138/am-2019-7054

Implications

None of the four investigated apatite solubility expressions can adequately explain the distribution of P_2O_5 concentrations from the entire suite of measured glassy melt inclusions and rehomogenized nanogranitoids. Current experimental models overestimate many of the concentrations of P_2O_5 in the analyzed melt inclusions and rehomogenized nanogranitoids, especially at high temperatures (Figs. 3, 4 and 6). This observation can be combined with other information from melt inclusions (e.g. Acosta-Vigil et al. 2010, 2017; Cesare et al. 2015; Bartoli et al. 2016) to understand the behavior of accessory minerals and partial melting mechanisms that operate during anatexis.

Although future experimental studies on apatite solubility in granitic melts may change these tentative conclusions, we have gained several important insights into apatite behavior in anatectic systems. Concentrations of P of nanogranites from relatively low temperature samples (e.g. Ronda, El Hoyazo) are mostly underestimated by apatite solubility expressions (except for the P92 solubility expression; Fig. 3), which suggests that melt may become locally saturated with respect to apatite even at low temperatures of melting. However, the concentration of P_2O_5 in the melt is probably controlled by compositional heterogeneity of the melt in anatectic systems (Fig. 9). At high temperatures (≥800-850 ºC), melt may become undersaturated in P_2O_5 due to exhaustion of apatite or apatite not being accessible (Bohemian massif, Kerala Khondalite, and maybe Barun, Kali Gandaki; Fig. 5).

Considering the discussion of the entire data set and the specific example of the El Hoyazo enclaves, inconsistencies between predicted and measured P_2O_5 concentrations are mostly explained by the exhaustion of apatite during high-temperature prograde metamorphism and problems with the current experimentally-derived solubility equations of apatite. One major

result from this study is realizing the need for more applicable experiments describing the solubility of apatite in strongly peraluminous and SiO_2-rich granite melts (Figure 7).

Apatite is an important repository for radiogenic trace elements used to infer the sources of granites. Apatite contains a large proportion of the REE budget of metapelites (Bea and Montero 1999; Ayres and Harris 1997; Acosta-Vigil et al. 2010), and apatite and monazite are estimated to host >99% of the Nd budget in a typical metapelite. Hence, the Nd isotope ratio of the melt will be mostly controlled by the dissolution and growth of these minerals and diffusion of Nd between these minerals and melt (e.g. Zeng et al. 2005). Neodymium isotopes signatures in apatite are generally homogenized at >500°C (Hammerli et al. 2014), but commonly preserve their initial signatures especially if they are included in major minerals (e.g. Janots et al. 2018). Apatite isotopic disequilibrium during anatexis has been proposed to account for Nd isotope values of granites that do not reflect that of their sources (e.g. Zeng et al. 2005).

Most nanogranitoid and melt inclusion sample suites have concentrations of P_2O_5 that are not systematically lower than the predicted apatite saturation values (Figs. 3 and 4), which is inconsistent with disequilibrium. In migmatites where apatite is expected to be in equilibrium with anatectic melt, Nd isotope values of apatite-saturated melts should have a compatible Nd isotope signature with their source rocks. This is generally observed in studies of consanguineous granulites and granites (e.g. Korhonen et al. 2010, 2015). If apatite is exhausted and monazite is still present, continued melting may not change the Nd isotopic signature of the melt as long as melt and monazite are in isotopic equilibrium. However, Nd isotope disequilibrium has been documented in the relatively low- to moderate-temperature Himalayan leucogranites (Ayres and Harris 1997). For the Himalayan samples from Kali Gandaki, P_2O_5 in most rehomogenized nanogranitoids are overestimated by the experimental models (Figure 3). The reasons for this is

781 unclear, but overestimation might be due to apatite disequilibrium, apatite
782 exhaustion/unavailability, or current solubility models not being appropriate. Therefore, Nd
783 isotope disequilibrium between crustal granites and their sources seems to be due to
784 unavailability of, and/or slow diffusion of Nd in the accessory minerals.

785 The concentrations of P_2O_5 in granites can be used to distinguish S-type and I-type
786 granites (London 1992; Sha and Chappell 1999). It is important to consider that apatite-
787 exhausted UHT metapelitic sources may generate melt that is undersaturated in P_2O_5 and these
788 granites may be misdiagnosed as I-type granites. Therefore, other discriminants should be used
789 in addition to P_2O_5 to distinguish different granite sources.

790

791 **Conclusions**

792 The concentrations of P_2O_5 in melt inclusions and nanogranitoids in peritectic minerals do not
793 show systematic changes with melt composition or temperature, which is generally inconsistent
794 with experimentally derived apatite solubility models. Comparison between predicted and
795 measured P_2O_5 concentrations indicate a strong influence of the ASI in the solubility of P_2O_5 in
796 melt, but also suggests that current models are not accurate enough and have limited predictive
797 capabilities for individual sample suites. Future experimental efforts are required to model the
798 solubility of apatite in granite melts. Apatite may become exhausted at high temperatures
799 especially in protoliths with low concentrations of P_2O_5 or with a high proportion of P-rich
800 silicate minerals. Phosphorus substitution into silicate minerals will deplete apatite during
801 prograde metamorphism and melt derived from high- to ultrahigh-temperature metamorphism
802 may be undersaturated in P_2O_5 relative to apatite due to apatite exhaustion and melt dilution.
803 This has implications for the Nd isotope ratios of and concentrations of P_2O_5 in of melt extracted

804 from the deep crust. More experimental work, particularly at high ASI and high SiO_2 values, is
805 needed to better quantify apatite solubility in anatectic systems. However, concentrations of P_2O_5
806 in rehomogenized nanogranitoids and glassy melt inclusions are generally expected to be close to
807 equilibrium values.
808

809 **Acknowledgements**

810 This research was partly funded by a Discovery Grant from the Natural Sciences and
811 Engineering Research Council of Canada. We thank R. Weinberg and J.C. Ayers and editor B.
812 Watson for constructive comments that greatly improved this manuscript.
813

814 **References**

815 Acosta-Vigil, A., Cesare, B., London, D., and Morgan, G.B. (2007) Microstructures and composition of
816 melt inclusions in a crustal anatectic environment, represented by metapelitic enclaves within El
817 Hoyazo dacites, SE Spain. Chemical Geology, 237, 450–465.
818 Acosta-Vigil, A., Buick, I., Hermann, J., Cesare, B., Rubatto, D., London, D., and Morgan, V.I.G.B.
819 (2010) Mechanisms of Crustal Anatexis: a Geochemical Study of Partially Melted Metapelitic
820 Enclaves and Host Dacite, SE Spain. Journal of Petrology, 51, 785–821.
821 Acosta-Vigil, A., Buick, I., Cesare, B., London, D., and Morgan, G.B., VI. (2012a) The Extent of
822 Equilibration between Melt and Residuum during Regional Anatexis and its Implications for
823 Differentiation of the Continental Crust: a Study of Partially Melted Metapelitic Enclaves.
824 Journal of Petrology, 53, 1319–1356.

825 Acosta-Vigil, A., London, D., and Morgan, G.B. (2012b) Chemical diffusion of major components in
826 granitic liquids: Implications for the rates of homogenization of crustal melts. Lithos, 153, 308–
827 323.
828 Acosta-Vigil, A., London, D., Morgan, G.B., Cesare, B., Buick, I., Hermann, J., and Bartoli, O. (2017)
829 Primary crustal melt compositions: Insights into the controls, mechanisms and timing of
830 generation from kinetics experiments and melt inclusions. Lithos, 286–287, 454–479.
831 Albarede, F. and Bottinga, Y. (1972). Kinetic disequilibrium in trace element partitioning between
832 phenocrysts and host lava. Geochimica et Cosmochimica Acta, 36, 141–156.
833 Ayres, M., and Harris, N. (1997) REE fractionation and Nd-isotope disequilibrium during crustal
834 anatexis: constraints from Himalayan leucogranites. Chemical Geology, 139, 249–269.
835 Baker, D.R. (2008). The fidelity of melt inclusions as records of melt composition. Contributions to
836 Mineralogy and Petrology, 156, 377–395.
837 Bartoli, O. (2017) Phase equilibria modelling of residual migmatites and granulites: An evaluation of the
838 melt-reintegration approach. Journal of Metamorphic Geology, 35, 919–942.
839 Bartoli, O., Cesare, B., Poli, S., Acosta-Vigil, A., Esposito, R., Turina, A., Bodnar, R.J., Angel, R.J., and
840 Hunter, J. (2013a) Nanogranite inclusions in migmatitic garnet: behavior during piston-cylinder
841 remelting experiments. Geofluids, 13, 405–420.
842 Bartoli, O., Cesare, B., Poli, S., Bodnar, R.J., Acosta-Vigil, A., Frezzotti, M.L., and Meli, S. (2013b)
843 Recovering the composition of melt and the fluid regime at the onset of crustal anatexis and S-
844 type granite formation. Geology, 41, 115–118.
845 Bartoli, O., Tajčmanová, L., Cesare, B., and Acosta-Vigil, A. (2013c) Phase equilibria constraints on
846 melting of stromatic migmatites from Ronda (S. Spain): insights on the formation of peritectic
847 garnet. Journal of Metamorphic Geology, 31, 775–789.

Bartoli, O., Cesare, B., Remusat, L., Acosta-Vigil, A., and Poli, S. (2014). The H2O content of granite embryos. Earth and Planetary Science Letters, 395, 281–290.

Bartoli, O., Acosta-Vigil, A., and Cesare, B. (2015) High-temperature metamorphism and crustal melting: working with melt inclusions. 2015, 84(3B).

Bartoli, O., Acosta-Vigil, A., Ferrero, S., and Cesare, B. (2016) Granitoid magmas preserved as melt inclusions in high-grade metamorphic rock. American Mineralogist, 101, 1543–1559.

Bea, F., Fershtater, G., and Corretgé, L. (1992) The geochemistry of phosphorus in granite rocks and the effect of aluminium. Lithos, 29, 43–56.

Bea, F. and Montero, P. (1999). Behavior of accessory phases and redistribution of Zr, REE, Y, Th, and U during metamorphism and partial melting of metapelites in the lower crust: an example from the Kinzigite Formation of Ivrea-Verbano, NW Italy. Geochimica et Cosmochimica Acta, 63, 1133–1153.

Bosse, V. and Villa, I.M. (2019). Petrochronology and hygrochronology of tectono-metamorphic events. Gondwana Research, 71, 76–90.

Brown, C.R., Yakymchuk, C., Brown, M., Fanning, C.M., Korhonen, F.J., Piccoli, P.M., and Siddoway, C.S. (2016) From Source to Sink: Petrogenesis of Cretaceous Anatectic Granites from the Fosdick Migmatite–Granite Complex, West Antarctica. Journal of Petrology, 57, 1241–1278.

Carosi, R., Montomoli, C., Langone, A., Turina, A., Cesare, B., Iaccarino, S., Fascioli, L., Visonà, D., Ronchi, A., and Rai, S.M. (2015) Eocene partial melting recorded in peritectic garnets from kyanite-gneiss, Greater Himalayan Sequence, central Nepal. Geological Society, London, Special Publications, 412, 111–129.

Cesare, B. (2008) Crustal melting: working with enclaves. Working with migmatites, 38, p. 37-55. Mineralogical Association of Canada Short Course Series.

Cesare, B. and Maineri, C. (1999). Fluid-present anatexis of metapelites at El Joyazo (SE Spain): constraints from Raman spectroscopy of graphite. Contributions to Mineralogy and Petrology, 135, 41–52.

Cesare, B., Acosta-Vigil, A. (2011). Using melt inclusions for understanding crustal melting processes. McGraw-Hill Yearbook of Science & Technology, 355–359.

Cesare, B., Salvioli-Mariani, E., Venturelli, G. (1997). Crustal anatexis and melt extraction during deformation in the restitic xenoliths at El Joyazo (SE Spain). Mineralogical Magazine, 61, 15–27.

Cesare, B., Marchesi, C., Hermann, J., and Gómez-Pugnaire, M.T. (2003) Primary melt inclusions in andalusite from anatectic graphitic metapelites: Implications for the position of the Al2SiO5 triple point. Geology, 31, 573–576.

Cesare, B., Maineri, C., Baron Toaldo, A., Pedron, D., and Acosta Vigil, A. (2007) Immiscibility between carbonic fluids and granitic melts during crustal anatexis: A fluid and melt inclusion study in the enclaves of the Neogene Volcanic Province of SE Spain. Chemical Geology, 237, 433–449.

Cesare, B., Ferrero, S., Salvioli-Mariani, E., Pedron, D., and Cavallo, A. (2009) "Nanogranite" and glassy inclusions: The anatectic melt in migmatites and granulites. Geology, 37, 627–630.

Cesare, B., Acosta-Vigil, A., Ferrero, S., Bartoli, O. and (2011). Melt inclusions in migmatites and granulites. In: Forster, M.A., Fitz Gerald, J.D. (Eds.), The Science of Microstructure – Part II. Journal of the Virtual Explorer Electronic Edition, ISSN 1441-8142, 38, paper 2.

Cesare, B., Acosta-Vigil, A., Bartoli, O., Ferrero, S. (2015). What can we learn from melt inclusions in migmatites and granulites? Lithos, 239, 186–216.

Chappel, B., and White, A. (2001) Two contrasting granite types: 25 years later. Australian Journal of Earth Sciences, 48, 489–499.

Clark, C., Fitzsimons, I.C.W., Healy, D., and Harley, S.L. (2011) How Does the Continental Crust Get Really Hot? Elements, 7, 235–240.

Corfu, F., and Stone, D. (1998) The significance of titanite and apatite U-Pb ages: constraints for the post-magmatic thermal-hydrothermal evolution of a batholithic complex, Berens River area, northwestern Superior Province, Canada. Geochimica et Cosmochimica Acta, 62, 2979–2995.

Dumond, G., Goncalves, P., Williams, M.L. and Jercinovic, M.J. (2015). Monazite as a monitor of melting, garnet growth and feldspar recrystallization in continental lower crust. Journal of Metamorphic Geology, 33, 735–762.

Engi, M. (2017). Petrochronology based on REE-minerals: monazite, allanite, xenotime, apatite. Reviews in Mineralogy and Geochemistry, 83, 365–418.

Farina, F., and Stevens, G. (2011) Source controlled 87 Sr/86 Sr isotope variability in granitic magmas: the inevitable consequence of mineral-scale isotopic disequilibrium in the protolith. Lithos, 122, 189–200.

Ferrero, S., Bartoli, O., Cesare, B., Salvioli-Mariani, E., Acosta-Vigil, A., Cavallo, A., Groppo, C., and Battiston, S. (2012) Microstructures of melt inclusions in anatectic metasedimentary rocks. Journal of Metamorphic Geology, 30, 303–322.

Ferrero, S., Bodnar, R.J., Cesare, B., and Viti, C. (2011) Re-equilibration of primary fluid inclusions in peritectic garnet from metapelitic enclaves, El Hoyazo, Spain. Lithos, 124, 117–131.

Ferrero, S., Braga, R., Berkesi, M., Cesare, B., and Laridhi Ouazaa, N. (2014) Production of metaluminous melt during fluid-present anatexis: an example from the Maghrebian basement, La Galite Archipelago, central Mediterranean. Journal of Metamorphic Geology, 32, 209–225.

916 Ferrero, S., Wunder, B., Walczak, K., O'Brien, P.J., and Ziemann, M.A. (2015) Preserved near
917 ultrahigh-pressure melt from continental crust subducted to mantle depths. Geology, 43, 447–
918 450.
919 Forshaw, J.B., Waters, D.J., Pattison, D.R.M., Palin, R.M., and Gopon, P. (2019) A comparison of
920 observed and thermodynamically predicted phase equilibria and mineral compositions in mafic
921 granulites. Journal of Metamorphic Geology, 37, 153–179.
922 Green, T.H. and Watson, E.B. (1982). Crystallization of apatite in natural magmas under high pressure,
923 hydrous conditions, with particular reference to 'orogenic'rock series. Contributions to
924 Mineralogy and Petrology, 791, 96–105.
925 Grunsky, E.C. (2010) The interpretation of geochemical survey data. Geochemistry: Exploration,
926 Environment, Analysis, 10, 27–74.
927 Hammerli, J., Kemp, A.I.S. and Spandler, C. (2014). Neodymium isotope equilibration during crustal
928 metamorphism revealed by in situ microanalysis of REE-rich accessory minerals. Earth and
929 Planetary Science Letters, 392, 133–142.
930 Harris, N., Vance, D., and Ayres, M. (2000) From sediment to granite: timescales of anatexis in the
931 upper crust. Chemical Geology, 162, 155–167.
932 Harrison, T.M., and Watson, E.B. (1984) The behavior of apatite during crustal anatexis: equilibrium
933 and kinetic considerations. Geochimica et Cosmochimica Acta, 48, 1467–1477.
934 Hermann, J., and Rubatto, D. (2003) Relating zircon and monazite domains to garnet growth zones: age
935 and duration of granulite facies metamorphism in the Val Malenco lower crust. Journal of
936 Metamorphic Geology, 21, 833–852.
937 Holtz, F., and Johannes, W. (1991) Genesis of Peraluminous Granites I. Experimental Investigation of
938 Melt Compositions at 3 and 5 kb and Various H2O Activities. Journal of Petrology, 32, 935–958.

939 Janots, E., Engi, M., Berger, A., Allaz, J., Schwarz, J.O. and Spandler, C. (2008). Prograde metamorphic
940 sequence of REE minerals in pelitic rocks of the Central Alps: implications for allanite–
941 monazite–xenotime phase relations from 250 to 610 C. Journal of Metamorphic Geology, 26,
942 509–526.
943 Johnson, T.E., Clark, C., Taylor, R.J., Santosh, M., and Collins, A.S. (2015) Prograde and retrograde
944 growth of monazite in migmatites: An example from the Nagercoil Block, southern India.
945 Geoscience Frontiers, 6, 373–387.
946 Kelsey, D.E., Clark, C. and Hand, M. (2008). Thermobarometric modelling of zircon and monazite
947 growth in melt - bearing systems: Examples using model metapelitic and metapsammitic
948 granulites. Journal of Metamorphic Geology, 26, 199‐212.
949 Kirkland, C.L., Yakymchuk, C., Szilas, K., Evans, N., Hollis, J., McDonald, B., and Gardiner, N.J.
950 (2018) Apatite: a U-Pb thermochronometer or geochronometer? Lithos, 318–319, 143–157.
951 Kohn, M.J. and Malloy, M.A. (2004). Formation of monazite via prograde metamorphic reactions
952 among common silicates: implications for age determinations. Geochimica et Cosmochimica
953 Acta, 68, 101–113.
954 Korhonen, F.J., Saito, S., Brown, M., Siddoway, C.S., and Day, J.M.D. (2010) Multiple Generations of
955 Granite in the Fosdick Mountains, Marie Byrd Land, West Antarctica: Implications for
956 Polyphase Intracrustal Differentiation in a Continental Margin Setting. Journal of Petrology, 51,
957 627–670.
958 Korhonen, F.J., Brown, M., Clark, C., Foden, J.D., and Taylor, R. (2015) Are granites and granulites
959 consanguineous? Geology, 43, 991–994.
960 London, D. (1992) Phosphorus in S-type magmas; the P 2 O 5 content of feldspars from peraluminous
961 granites, pegmatites, and rhyolites. American Mineralogist, 77(, 126–145.

London, D., Morgan, G.B., Babb, H.A., and Loomis, J.L. (1993) Behavior and effects of phosphorus in the system Na2O−K2O−Al2O3−SiO2−P2O5−H2O at 200 MPa(H2O). Contributions to Mineralogy and Petrology, 113, 450–465.

London, D., Wolf, M.B., Morgan, G.B., and Garrido, M.G. (1999) Experimental silicate–phosphate equilibria in peraluminous granitic magmas, with a case study of the Alburquerque batholith at Tres Arroyos, Badajoz, Spain. Journal of Petrology, 40, 215–240.

London, D., Morgan, G.B., and Acosta-Vigil, A. (2012) Experimental simulations of anatexis and assimilation involving metapelite and granitic melt. Lithos, 153, 292–307.

Morgan, G.B., and London, D. (2005a) Effect of current density on the electron microprobe analysis of alkali aluminosilicate glasses. American Mineralogist, 90, 1131–1138.

Mysen, B.O. (1998) Phosphorus solubility mechanisms in haplogranitic aluminosilicate glass and melt: effect of temperature and aluminum content. Contributions to Mineralogy and Petrology, 133, 38–50.

Mysen, B.O., Ryerson, F.J., and Virgo, D. (1981) The structural role of phosphorus in silicate melts. American Mineralogist, 66, 106–117.

Nandakumar, V., & Harley, S. L. (2019). Geochemical signatures of mid-crustal melting processes and heat production in a hot orogen: The Kerala Khondalite Belt, Southern India. Lithos, 324, 479–500.

Palarea-Albaladejo, J., and Martín-Fernández, J.A. (2013) Values below detection limit in compositional chemical data. Analytica Chimica Acta, 764, 32–43.

Palarea-Albaladejo, J., and Martín-Fernández, J.A. (2015) zCompositions — R package for multivariate imputation of left-censored data under a compositional approach. Chemometrics and Intelligent Laboratory Systems, 143, 85–96.

985 Pan, Y., and Fleet, M.E. (2002) Compositions of the Apatite-Group Minerals: Substitution Mechanisms
986 and Controlling Factors. Reviews in Mineralogy and Geochemistry, 48, 13–49.
987 Pattison, D.R., De Capitani, C., and Gaidies, F. (2011) Petrological consequences of variations in
988 metamorphic reaction affinity. Journal of Metamorphic Geology, 29, 953–977.
989 Piccoli, P.M., and Candela, P.A. (2002) Apatite in igneous systems. Reviews in Mineralogy and
990 Geochemistry, 48, 255–292.
991 Pichavant, M., Montel, J.-M., and Richard, L.R. (1992) Apatite solubility in peraluminous liquids:
992 Experimental data and an extension of the Harrison-Watson model. Geochimica et
993 Cosmochimica Acta, 56, 3855–3861.
994 Pyle, J.M. and Spear, F.S. (1999). Yttrium zoning in garnet: coupling of major and accessory phases
995 during metamorphic reactions. Geological Materials Research, 1, 1–49.
996 Roedder, E. (1984). Fluid Inclusions. Reviews in Mineralogy 12, 1–644.
997 Sawyer, E.W. (1987) The Role of Partial Melting and Fractional Crystallization in Determining
998 Discordant Migmatite Leucosome Compositions. Journal of Petrology, 28, 445–473.
999 Sawyer, E.W. (2008) Atlas of migmatites. NRC Research Press, Ottawa. pp 387.
1000 Sha, L.K. and Chappell, B.W. (1999). Apatite chemical composition, determined by electron microprobe
1001 and laser-ablation inductively coupled plasma mass spectrometry, as a probe into granite
1002 petrogenesis. Geochimica et Cosmochimica Acta, 63, 3861–3881.
1003 Shrestha, S., Larson, K.P., Duesterhoeft, E., Soret, M. and Cottle, J.M. (2019). Thermodynamic
1004 modelling of phosphate minerals and its implications for the development of PTt histories: A
1005 case study in garnet-monazite bearing metapelites. Lithos 334, 141–160.
1006 Spear, F.S. (2010) Monazite–allanite phase relations in metapelites. Chemical Geology, 279, 55–62.

1007 Spear, F.S. and Pyle, J.M. (2002). Apatite, monazite, and xenotime in metamorphic rocks. Reviews in
1008 Mineralogy and Geochemistry, 48, 293–335.
1009 Spear, F.S., and Pyle, J.M. (2010) Theoretical modeling of monazite growth in a low-Ca metapelite.
1010 Chemical Geology, 273, 111–119.
1011 Stepanov, A.S., Hermann, J., Rubatto, D., and Rapp, R.P. (2012) Experimental study of monazite/melt
1012 partitioning with implications for the REE, Th and U geochemistry of crustal rocks. Chemical
1013 Geology, 300, 200–220.
1014 Tollari, N., Toplis, M.J., and Barnes, S.J. (2006) Predicting phosphate saturation in silicate magmas: An
1015 experimental study of the effects of melt composition and temperature. Geochimica et
1016 Cosmochimica Acta, 70, 1518–1536.
1017 Toplis, M., and Dingwell, D. (1996) The variable influence of P 2 O 5 on the viscosity of melts of
1018 differing alkali/aluminium ratio: Implications for the structural role of phosphorus in silicate
1019 melts. Geochimica et Cosmochimica Acta, 60, 4107–4121.
1020 Villaros, A., Stevens, G., Moyen, J.-F., and Buick, I.S. (2009) The trace element compositions of S-type
1021 granites: evidence for disequilibrium melting and accessory phase entrainment in the source.
1022 Contributions to Mineralogy and Petrology, 158, 543–561.
1023 Villaseca, C., Romera, C.M., De la Rosa, J. and Barbero, L. (2003). Residence and redistribution of
1024 REE, Y, Zr, Th and U during granulite-facies metamorphism: behaviour of accessory and major
1025 phases in peraluminous granulites of central Spain. Chemical Geology, 200, 293–323.
1026 Watson, E.B. (1979) Apatite saturation in basic to intermediate magmas. Geophysical Research Letters,
1027 6, 937–940.
1028 Watson, E.B. (1980). Apatite and phosphorus in mantle source regions: an experimental study of
1029 apatite/melt equilibria at pressures to 25 kbar. Earth and Planetary Science Letters, 51, 322–335.

1030 Watson, E.B., and Green, T.H. (1981) Apatite/liquid partition coefficients for the rare earth elements
1031 and strontium. Earth and Planetary Science Letters, 56, 405–421.
1032 Watt, G.R. and Harley, S.L. (1993). Accessory phase controls on the geochemistry of crustal melts and
1033 restites produced during water-undersaturated partial melting. Contributions to Mineralogy and
1034 Petrology, 114, 550–566.
1035 Webster, J.D., and Piccoli, P.M. (2015) Magmatic apatite: a powerful, yet deceptive, mineral. Elements,
1036 11, 177–182.
1037 Weinberg, R.F. (2016) Himalayan leucogranites and migmatites: nature, timing and duration of anatexis.
1038 Journal of Metamorphic Geology, 34, 821–843.
1039 White, R.W., Stevens, G., and Johnson, T.E. (2011) Is the crucible reproducible? Reconciling melting
1040 experiments with thermodynamic calculations. Elements, 7, 241–246.
1041 Wolf, M.B. and London, D. (1994). Apatite dissolution into peraluminous haplogranitic melts: an
1042 experimental study of solubilities and mechanisms. Geochimica et Cosmochimica Acta, 58,
1043 4127–4145.
1044 Wolf, M.B. and London, D. (1995). Incongruent dissolution of REE-and Sr-rich apatite in peraluminous
1045 granitic liquids: Differential apatite, monazite, and xenotime solubilities during anatexis.
1046 American Mineralogist, 80, 765–775.
1047 Wolfram, L.C., Weinberg, R.F., Hasalová, P. and Becchio, R. (2017). How Melt Segregation Affects
1048 Granite Chemistry: Migmatites from the Sierra de Quilmes, NW Argentina. Journal of Petrology,
1049 58, 2339–2364.
1050 Yakymchuk, C. (2017) Behaviour of apatite during partial melting of metapelites and consequences for
1051 prograde suprasolidus monazite growth. Lithos, 274–275, 412–426.

1052 Yakymchuk, C., and Brown, M. (2014) Consequences of open-system melting in tectonics. Journal of
1053 the Geological Society, 171, 21–40.
1054 Yakymchuk, C., and Brown, M. (2019) Divergent behaviour of Th and U during anatexis: Implications
1055 for the thermal evolution of orogenic crust. Journal of Metamorphic Geology.
1056 https://doi.org/10.1111/jmg.12469
1057 Yakymchuk, C., Clark, C., and White, R.W. (2017) Phase Relations, Reaction Sequences and
1058 Petrochronology. Reviews in Mineralogy and Geochemistry, 83, 13–53.
1059 Yakymchuk, C., Kirkland, C.L., and Clark, C. (2018) Th/U ratios in metamorphic zircon. Journal of
1060 Metamorphic Geology, 36, 715–737.
1061 Yakymchuk, C., Zhao, W., Wan, Y., Lin, S., and Longstaffe, F.J. (2019). Fluid-present anatexis of
1062 Neoarchean tonalite and amphibolite in the Western Shandong Province. Lithos, 326–327, 110–
1063 124.
1064 Zeck, H.P., Williams, I., 2002. Inherited and magmatic zircon from Neogene Hoyazo cordierite dacite,
1065 SE Spain-Anatectic source rock provenance and magmatic evolution. Journal of Petrology 43,
1066 1089–1104.
1067 Zeng, L., Saleeby, J.B., and Asimow, P. (2005) Nd isotope disequilibrium during crustal anatexis: A
1068 record from the Goat Ranch migmatite complex, southern Sierra Nevada batholith, California.
1069 Geology, 331, 53–56.
1070 Zhang, Y., Ni, H., Chen, Y. (2010). Diffusion data in silicate melts. In: Zhang, Y., Cherniak, D.J.
1071 (Eds.), Diffusion in Minerals and Melts. Reviews in Mineralogy and Geochemistry 72,
1072 311–408.
1073
1074

This is a preprint, the final version is subject to change, of the American Mineralogist (MSA)
Cite as Authors (Year) Title. American Mineralogist, in press.
DOI: https://doi.org/10.2138/am-2019-7054

Figure captions

Figure 1. *P–T* diagram showing the approximate metamorphic conditions recorded by trapped nanogranitoids and melt inclusions and the *P–T* conditions of experimental runs. The El Hoyazo samples represent melt inclusions in peritectic garnet in enclaves and the other samples represent rehomogenized nanogranitoid and glassy melt inclusions hosted by garnet in migmatites and granulites. Experimental studies: WL: Wolf and London (1994), P92: Pichavant et al. (1992), GW82: Green and Watson (1982). HW: Harrison and Watson (1984), W80: Watson (1980). KKB: Kerala Khondalite Belt.

Figure 2. Concentration of P_2O_5 in nanogranitoids (data from Bartoli et al. 2016) as a function of the concentration of SiO_2 in melt and the ASI value of the melt. Nanogranitoid compositions are compared with the results of apatite solubility models (dashed lines) of Harrison and Watson (1984; HW84) and Wolf and London (1994; WL94). Ronda1 have homogenization temperatures of 660–700°C whereas Ronda2 have homogenization temperatures of ~850°C (see Bartoli et al. 2016).

Figure 3. Concentration of the measured P_2O_5 of glassy melt inclusions and rehomogenized nanogranitoid versus the predicted P_2O_5 concentrations using various apatite solubility expressions, major element compositions (SiO_2, Al_2O_3, Na_2O, K_2O and CaO measured with electron probe microanalysis), and estimated temperatures of entrapment of individual rehomogenized nanogranitoids and glassy melt inclusions. Solubility expressions are from: **(a)** HW84: Harrison and Watson (1984), **(b)** B92: Bea et al. (1992), **(c)** P92: Pichavant et al. (1992), and **(d)** WL94: Wolf and London (1994). The red line illustrates where the predicted and

measured compositions are the same. For (d), some results are not included (La Galite and some data from the Bohemian Massif) because they have aluminum saturation values <1.1 that are outside the calibration range of the WL94 expression. Most P_2O_5 values are underestimated by the HW84 and B92 expressions. Ronda1 have homogenization temperatures of 660–700°C whereas Ronda2 have homogenization temperatures of ~850°C (see Bartoli et al. 2016).

Figure 4. Log-normalized histograms of the quotient of the measured concentration of P_2O_5 in nanogranitoid inclusions divided by the P_2O_5 concentration in melt predicted from various solubility expressions using the measured compositions of SiO_2, Al_2O_3, Na_2O, K_2O and CaO and estimated temperatures of entrapment of individual rehomogenized nanogranites and glassy melt inclusions. **(a)** HW84: Harrison and Watson (1984), **(b)** B92: Bea et al. (1992), **(c)** P92: Pichavant et al. (1992), and **(d)** WL94: Wolf and London (1994). Most of the nanogranite inclusions measured from the Barun gneiss have ASI (aluminum saturation index) values of < 1.1 and are not plotted in (d).

Figure 5. Box-and-whisker plot of the P_2O_5 concentrations in nanogranitoids from different locations arranged by approximate entrapment temperatures (from Bartoli et al. 2016). On the box-and-whisker plots, the whiskers extend to the lowest and highest datum inside 1.5 times the interquartile range and outliers (represented by crosses) are outside of this range. The number of data points are shown in italics above each box. Samples from the highest temperature samples have the lowest concentrations of P_2O_5, with the exception of the La Galite metatonalite samples.

Figure 6. Amount of apatite remaining relative to the amount at the solidus as a function of *P–T* for an average metapelite (modified from Yakymchuk, 2017). The bulk rock composition is 0.10 wt.% P_2O_5. Red dots represent the approximate *P–T* conditions from samples with measured nanogranitoid and melt inclusion compositions.

Figure 7. Schematic diagram illustrating how the concentration of P_2O_5 in melt is expected to increase with *T* until apatite is completely exhausted (or removed from the system as inclusions). After this point, further melting will dilute the melt in P_2O_5.

Figure 8. Difference between measured concentration of P_2O_5 (wt.%) and concentrations predicted by various apatite solubility models combined with measured concentrations of major elements and estimated entrapment temperatures of individual melt inclusions in the El Hoyazo enclaves. **(a)** Difference between measured and predicted concentrations of P_2O_5 versus Aluminium Saturation Index (ASI). **(b)** Difference between measured and predicted concentrations of P_2O_5 versus wt.% SiO_2

Figure 9. Compositions of melt inclusions in plagioclase and garnet from the El Hoyazo enclaves. Concentrations of P_2O_5 in the melt inclusions are slightly higher in garnet (about 0.1 wt.%), Al_2O_3 is slightly lower in melt inclusions in plagioclase (2 wt.%) but, SiO_2 is slightly higher in melt inclusions in plagioclase (2 wt.%).

This is a preprint, the final version is subject to change, of the American Mineralogist (MSA)
Cite as Authors (Year) Title. American Mineralogist, in press.
DOI: https://doi.org/10.2138/am-2019-7054

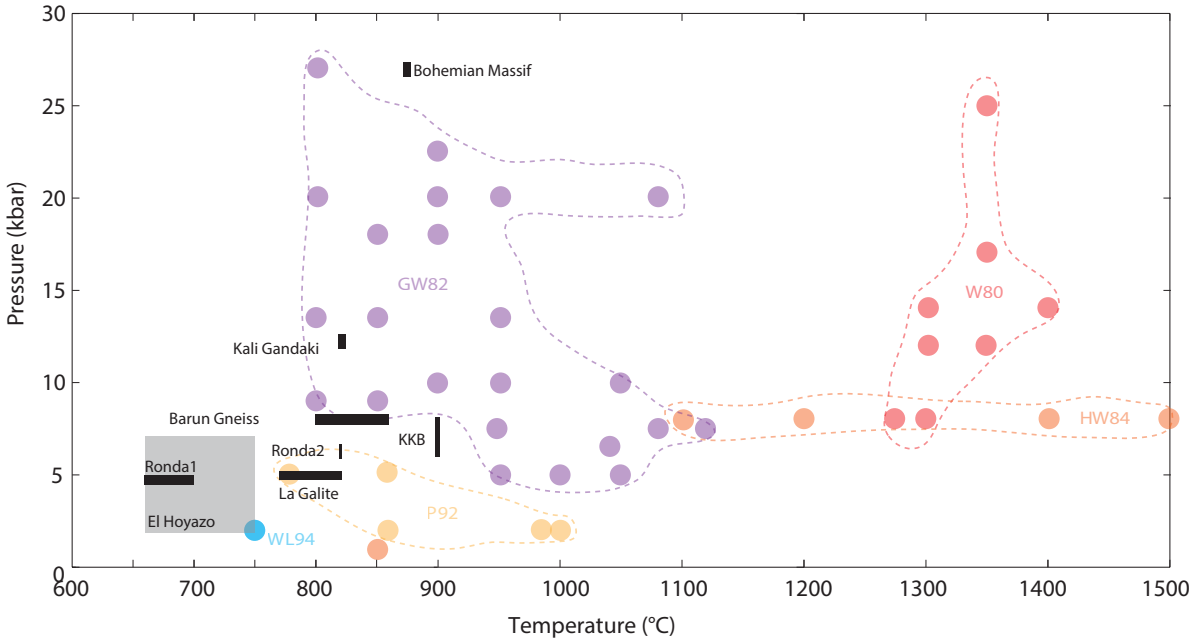

Figure 1

This is a preprint, the final version is subject to change, of the American Mineralogist (MSA)
Cite as Authors (Year) Title. American Mineralogist, in press.
DOI: https://doi.org/10.2138/am-2019-7054

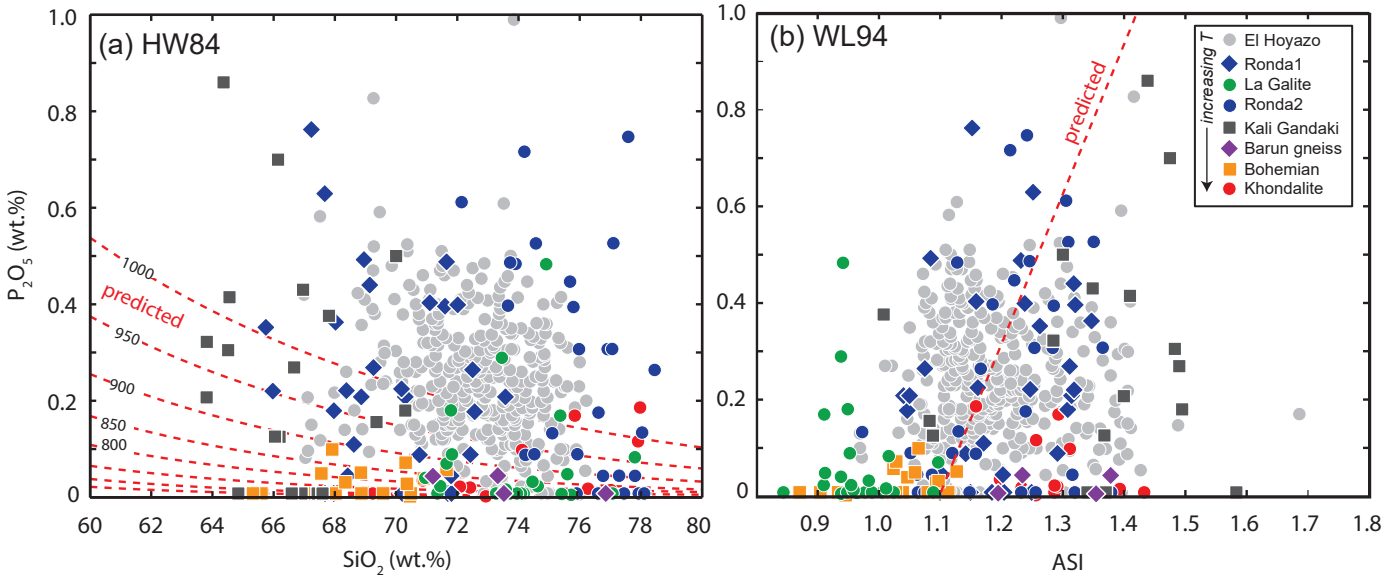

Figure 2

This is a preprint, the final version is subject to change, of the American Mineralogist (MSA)
Cite as Authors (Year) Title. American Mineralogist, in press.
DOI: https://doi.org/10.2138/am-2019-7054

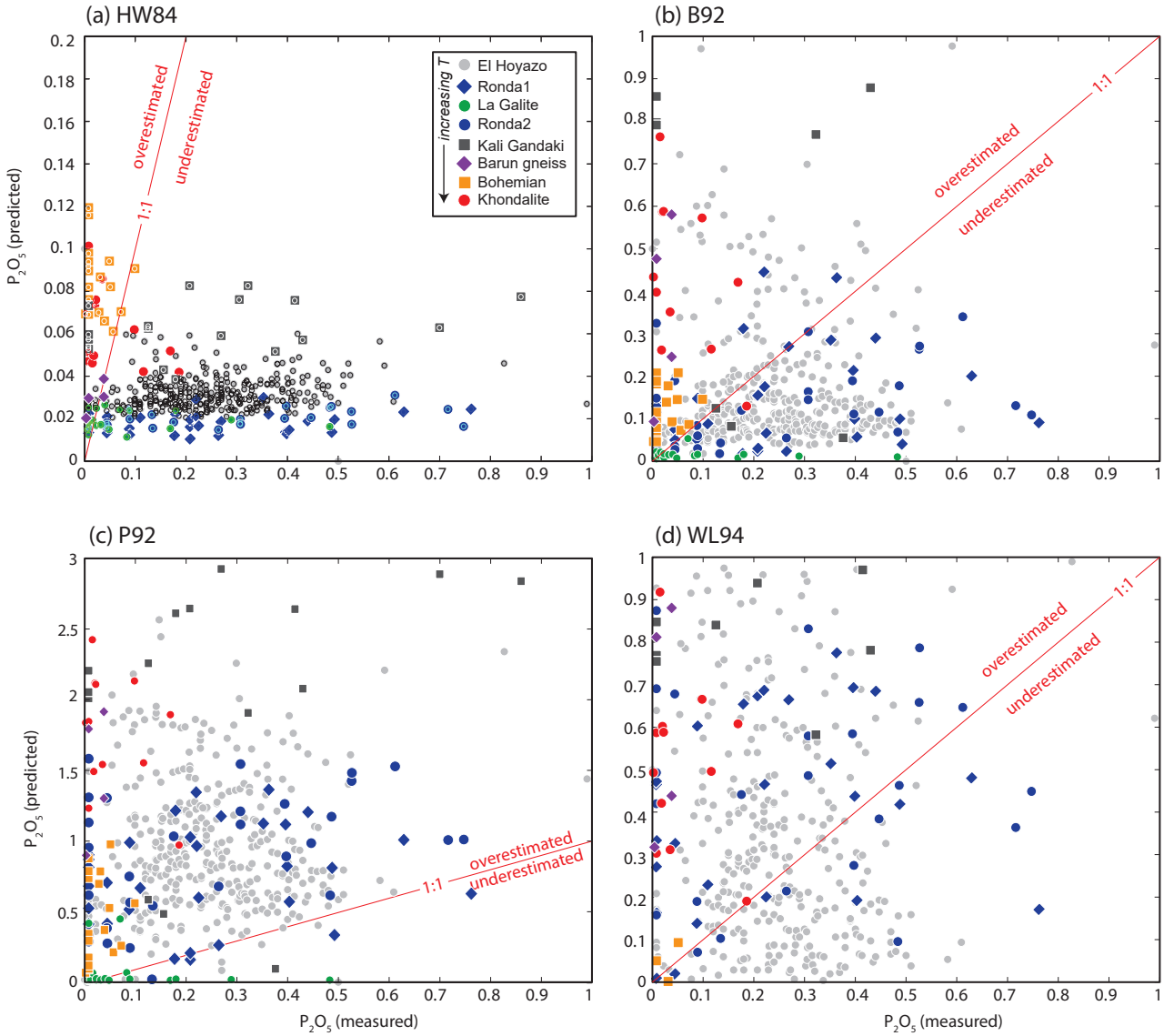

Figure 3

This is a preprint, the final version is subject to change, of the American Mineralogist (MSA)
Cite as Authors (Year) Title. American Mineralogist, in press.
DOI: https://doi.org/10.2138/am-2019-7054

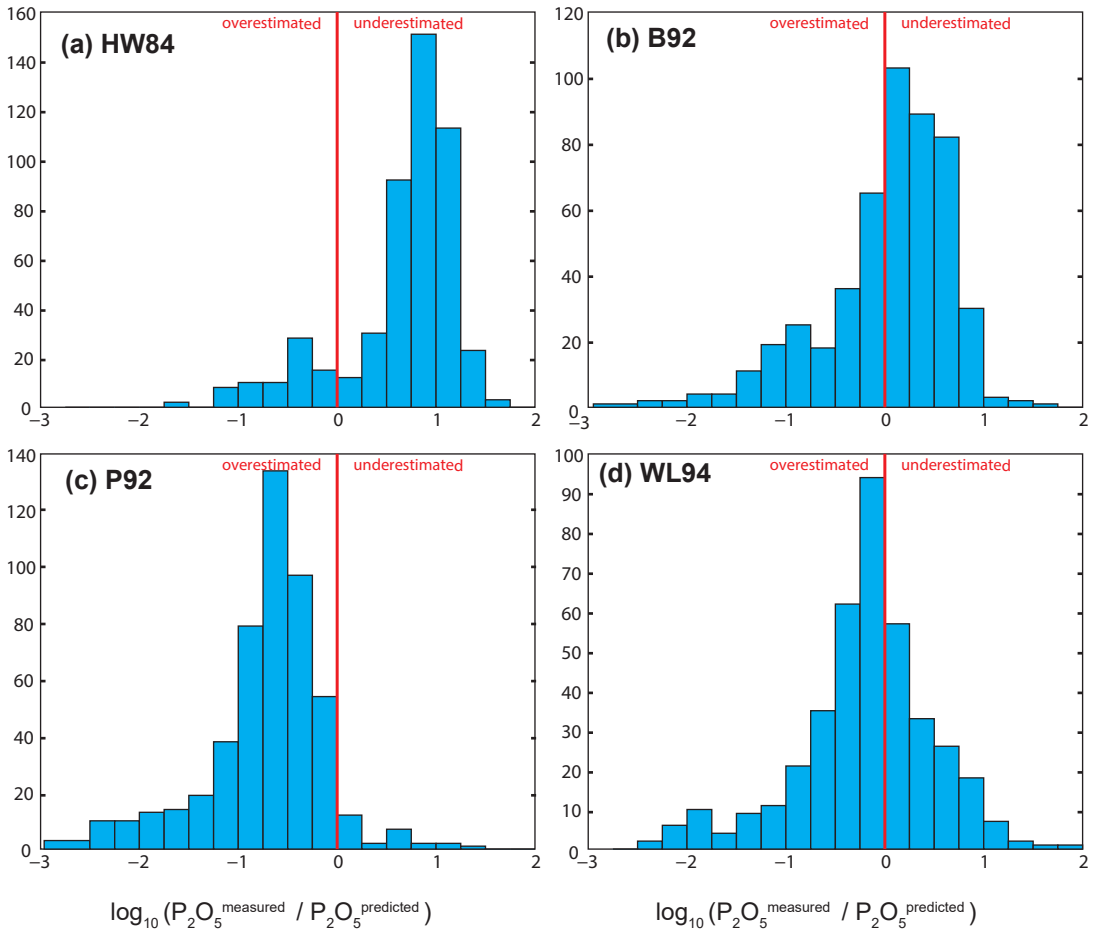

Figure 4

This is a preprint, the final version is subject to change, of the American Mineralogist (MSA)
Cite as Authors (Year) Title. American Mineralogist, in press.
DOI: https://doi.org/10.2138/am-2019-7054

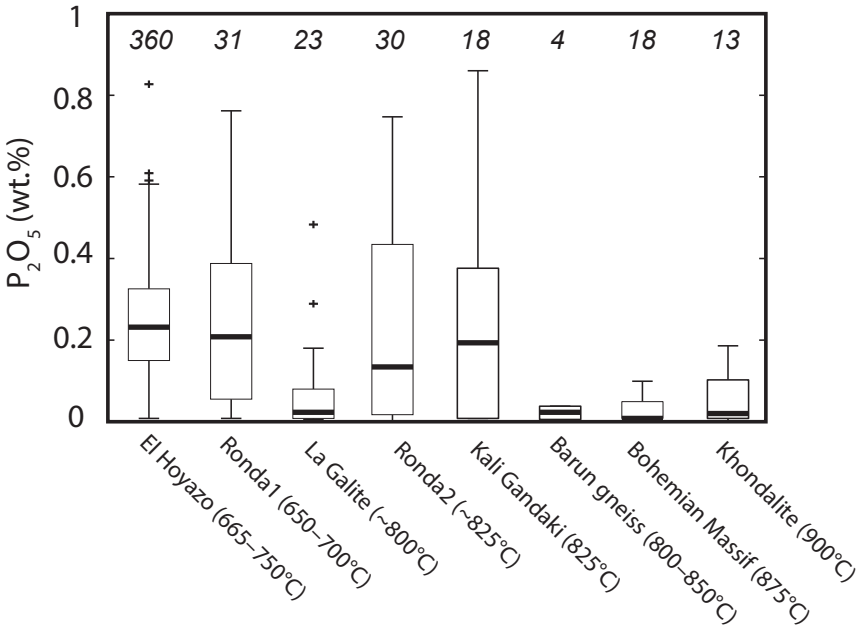

Figure 5

This is a preprint, the final version is subject to change, of the American Mineralogist (MSA)
Cite as Authors (Year) Title. American Mineralogist, in press.
DOI: https://doi.org/10.2138/am-2019-7054

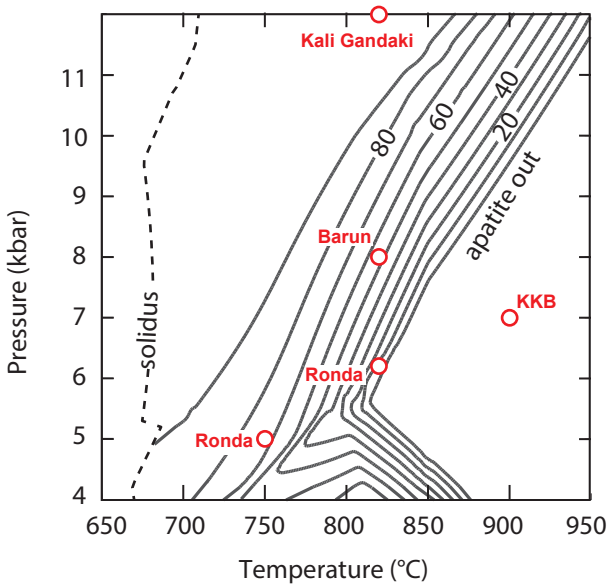

Figure 6

This is a preprint, the final version is subject to change, of the American Mineralogist (MSA)
Cite as Authors (Year) Title. American Mineralogist, in press.
DOI: https://doi.org/10.2138/am-2019-7054

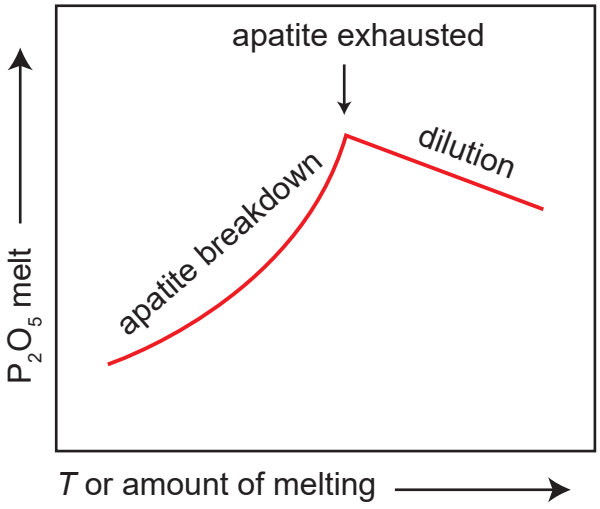

Figure 7

This is a preprint, the final version is subject to change, of the American Mineralogist (MSA)
Cite as Authors (Year) Title. American Mineralogist, in press.
DOI: https://doi.org/10.2138/am-2019-7054

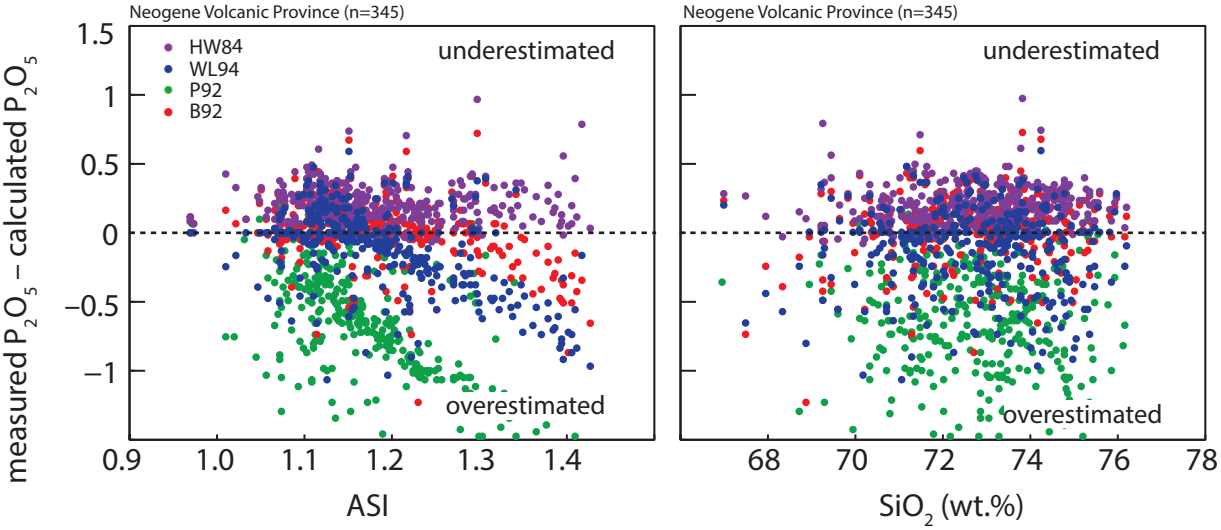

Figure 8

This is a preprint, the final version is subject to change, of the American Mineralogist (MSA)
Cite as Authors (Year) Title. American Mineralogist, in press.
DOI: https://doi.org/10.2138/am-2019-7054

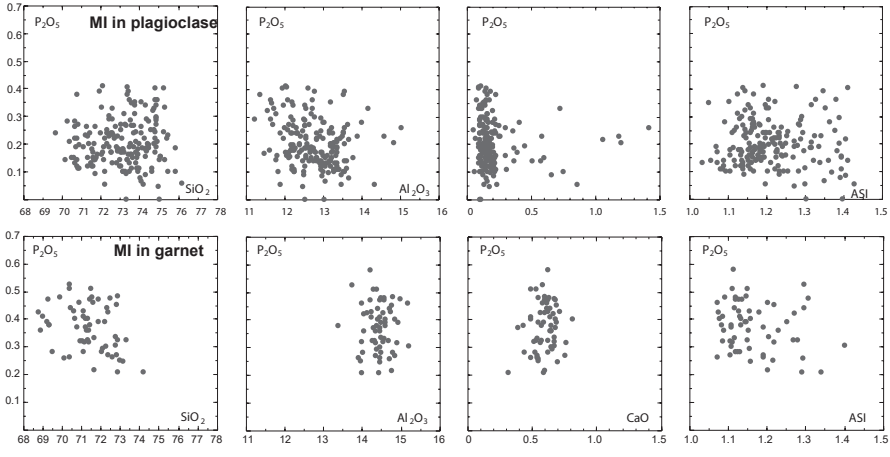

Figure 9